# Transparent and High Gain Screens Based on Microlens Arrays for Projection Displays

**by**

**Mehmet Kıvanç Hedili**

**A Thesis Submitted to the**
**Graduate School of Sciences and Engineering**
**in Partial Fulfillment of the Requirements for**
**the Degree of**

**Master of Science**

**in**

**Electrical and Electronics Engineering**

**Koç University**

**July 2013**

Koç University
Graduate School of Sciences and Engineering

This is to certify that I have examined this copy of a master's thesis by

Mehmet Kıvanç Hedili

and have found that it is complete and satisfactory in all respects,
and that any and all revisions required by the final
examining committee have been made.

Committee Members:

_____
Prof. Dr. Hakan Ürey

_____
Assoc. Prof. Göksen Göksenin Yaralıoğlu

_____
Asst. Prof. Şükrü Ekin Kocabaş

Date: 23.07.2013

## ABSTRACT

Tablet computers and smart phones have increased the mobility of the users but small screen size has been a major limitation for the productivity of the users. Mobile projectors, called pico-projectors, are emerging technologies and can project images to any distance and size from a tiny display engine that can be embedded in mobile computers and phones. While pico-projectors can overcome the screen size limitation, they are limited in brightness due to battery operation and laser safety concerns. The aim of this research was to develop reflective and transparent novel screen technologies that can provide high-efficiency and high-brightness when used together with laser scanning based pico-projectors. Such screens are needed in augmented reality displays, head-up displays, and head-mounted projection displays. When an image is projected on ordinary surfaces, such as walls or a piece of paper, the light is scattered onto the entire hemisphere. We developed special micro-structured screens that concentrate the scattered light only around the user's eyes. As the projected energy is concentrated into a smaller area, the brightness of the image is increased and the screen has a gain compared to ordinary surfaces.

Three different screen technologies have been developed that use microlens array (MLA) based diffusers: a single MLA screen, a dual MLA screen and a rotated MLA screen. The single MLA screen has a gain of 3 and it was designed for automotive head-up display applications. Due to its unique index matched structure the screen provides excellent transparency and high brightness at the same time. The dual MLA screen is an opaque screen with a gain of 9. It concentrates the diffused light more efficiently compared to the single MLA due to the telecentricity of the microlenses. A novel rotated MLA provides the highest gain of all the screens. It is designed specifically for a given

application such that every pixel on the screen is reflected towards the user due to the rotation of the microlenses. It can provide gains on the order of 100.

# ÖZET

Tablet bilgisayarlar ve akıllı telefonlar kullanıcının hareket kabiliyetini arttırmaktadır ancak küçük ekranları kullanıcı açısından önemli bir kısıtlayıcı etken olmaktadır. Piko-projektör adı verilen taşınabilir projektörler, bu cihazların içine gömülerek istenilen uzaklıkta ve büyüklükte görüntü yansıtılmasına olanak tanımaktadır. Elde taşınabilir projektörler ekran büyüklüğü sorununu çözmekle birlikte pille çalışmaları ve lazer güvenliği gereği çıkış güçleri düşük olduğundan istenilen parlaklıkta görüntü üretememektedirler. Bu araştırmanın amacı lazer piko-projektörlerle kullanıldığında yüksek verim ve parlaklık sağlayan, özgün şeffaf ve opak ekran teknolojilerinin geliştirilmesidir. Bu ekranlara augmented reality, head-up display ve head-mounted display gibi uygulamalar için gerek duyulmaktadır. Duvar, kağıt gibi sıradan yüzeylere projeksiyon yapıldığında ışık bütün yarıküreye dağıtılır. Yansıtılan ışığı yalnızca kullanıcının gözleri çevresine dağıtan özel bir mikro yapılı ekran geliştirilmiştir. Projektörün çıkış enerjisi daha küçük bir alana yoğunlaştırıldığından daha parlak görüntü elde edilmektedir ve ekranın sıradan yüzeylere göre kazancı vardır.

Mikromercek dizinleri (MMD) kullanılarak üç farklı tasarım yapılmıştır: tek katman MMD, çift takman MMD ve döndürülmüş MMD. Otomobillerde head-up display uygulaması için geliştirilen tek katman MMD ekranının kazancı 3'tür. Eşleştirilmiş kırınım ideksi yapısı sayesinde ekran hem çok iyi şeffaflık hemde çok parlak görüntü sağlamaktadır. Çift katman MMD ışınları optik eksene paralel hale getirdiği için yayılan ışığı daha verimli bir şekilde yağunlaştırır. Tasarlanan ekranın kazancı 9'dur. Özgün olarak tasarlanan döndürülmüş mikromerceklerden oluşan ekran ile çok yüksek kazançlar elde etmek mümkündür. Uygulamaya özel olarak tasarlanan ekranlar her mikromerceğin kendine özel döndürülme açıları nedeniyle her pikseli kullanıcıya doğru çok verimli bir

şekilde yönlendirir. Bu teknolojiyle ekran kazancını 100'ler mertebesine çıkarmak mümkündür.

## ACKNOWLEDGEMENT

I would like to thank Prof. Hakan Ürey for letting me study in such a productive research environment as OML. His constructive comments and creative ideas paved the way to this exciting and fruitful research. I would also like to thank Mark Freeman for being my co-advisor during my MS studies and my internship at Microvision. I am also thankful to Microvision Inc. for sponsoring this research and for giving me an opportunity to do an internship in the company prior to my MS research. It would have been impossible to complete my studies without the help of my colleagues and good friends at OML. I am also thankful to Prof. Göksenin Yaralıoğlu and Prof. Şükrü Ekin Kocabaş for taking part in my thesis committee.

Last but not least, I am deeply grateful to my family for doubtlessly believing in me. I would not be able to complete this thesis without the support of my family to whom I dedicate it.

## LIST OF FIGURES

# Table of Contents

# 1 INTRODUCTION

A screen is a device that diffuses the incident light onto a large space so that the image projected onto it can be seen from a larger area. There are many types of diffusers: random diffusers, diffractive optical element (DOE) based diffusers, microlens array (MLA) based diffusers, etc. Most of the surfaces can be considered as random diffusers such as walls, a piece of paper or projection screens in the conference rooms. They diffuse the light uniformly in every direction within a hemisphere so the image can be seen from anywhere in front of the screen [1]. DOE based screens are generally composed of periodic microstructures so that incident light is split into diffraction orders that contain the full information for each pixel on the screen [21]. The surface structure can be modified to control the diffuser angle. With MLA based screens each pixel of the display is expanded by a microlens and the size of the expansion is controlled by the numerical aperture o the microlenses, which can be easily manipulated in the design stage [19].

With Lambertian diffusers there is not much control over the size of the reflection cone, whereas with DOE and MLA based diffusers the size of the reflection cone can be controlled. That reflection cone is called the eyebox. The eyebox is defined as a virtual window hanging in the air, from which the content on the screen can be seen by the user [23]. For example, the eyebox for the random diffuser screen is the entire hemisphere. With MLA based screens the eyebox size is determined by the divergence angle of the marginal rays, whereas with DEO based screens the eyebox size is set by the designer and a computer generated microstructure is created, which yields the desired eyebox characteristics.

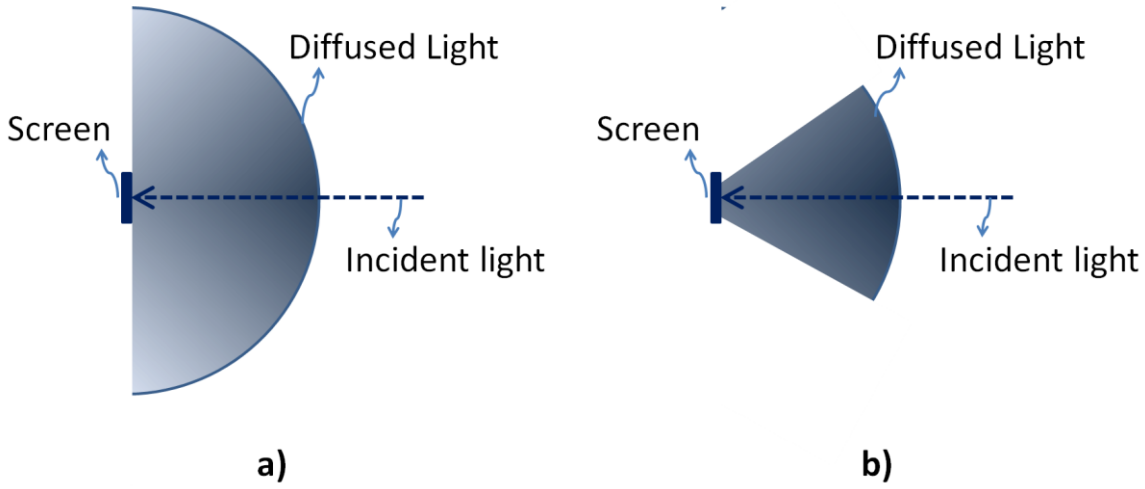


Figure 1.1: a) A Lambertian scatterer diffuses the incident light in every direction in a hemisphere. b) A screen that has a gain concentrates the diffused light in a smaller area.

The eyebox size determines the brightness of the screen. Each pixel on the screen has its own eyebox and the overlapped region of those individual eyeboxes determines the usable eyebox, from where the whole image can be seen. By concentrating the output power of the projector in the overlapped eyebox the perceived brightness can be increased compared to a Lambertian scatterer (i.e. same power in a smaller area) as illustrated in Figure 1.1. This relative increase in brightness compared to a Lambertian scatterer is called the gain of the screen. For example, a gain of 2 means for the same projector the image is twice as bright compared to a Lambertian screen; or, from another perspective, the image has the same brightness with a Lambertian screen that is projected with a2 times more powerful projector. Invention of portable, hand-held pico-projectors, which is planned to be embedded in cell phones in the future, requires high gain screens because of their low power output due to eye safety reasons.

Figure 1.2: The effect of speckle can be seen on the left compared to the speckle-compensated image on the right [2].

The most successful pico-projectors in the market are laser based, which use three different wavelength lasers to project color images: Red, Green and Blue. Among the diffuser technologies described above using MLA based screens with laser projectors is a better option. As the name suggests, random diffusers have a rough surface profile and the sub-wavelength random variations across the screen causes random interference patterns when illuminated with coherent light, such as lasers, which is called speckle, that looks like pepper noise on the image as seen in Figure 1.2 [2]. Moreover their eyebox size is not controllable which means high gain random diffuser screens cannot be made. DOE based screens work well with monochromatic projectors but for color laser projectors the eyebox size scales with wavelength, which results in poor color balance across the eyebox [21]. MLA based screens have been proven to work with color projectors [19][20]. The eyebox size is determined by the f/# of the microlenses so it is independent of the wavelength, which provides excellent color balance across the eyebox. Since the microlenses are

fabricated with good optical quality the random variations across the screen are negligible, thus the screen has virtually no speckle which is particularly important with laser projectors. Moreover, the size and the shape of the eyebox can be easily controlled by the f/# and the aperture size of the microlenses, respectively. As a result MLA technology has been selected as the basis for designing high gain projection screens.

Table 1.1: Design parameters

| Display Parameters | Screen Parameters |
|---|---|
| Brightness | Radius of curvature |
| Eyebox size | MLA pitch |
| Image quality | Gain |

In this thesis three different microlens array based screen technologies are presented with different display and screen parameters as shown in Table 1.1. In Section 2 a single MLA based transparent augmented reality display is presented, which has a gain of about 3. The design methodology, transparent MLA screen operation principle, simulations and experimental results are discussed. In Section 3 a reflective dual MLA screen is presented, which has a gain of about 9. Operation theory and simulation results are compared to the single MLA case and experimental results are shown. In Section 4 a novel rotated MLA screen design is presented which has a gain of about 100. The design methodology for such a screen and simulations are presented as a case study of a direct projection automotive HUD system.

## 1.1 Contributions of the Thesis

Main contributions of this thesis are in the design methodology of high gain MLA based screens. In the transparent single MLA screen the constraints on the MLA specifications

have been addressed and published in Ref [19]. We showed that the transparent single MLA screen combined with a laser projector can be used as a direct projection head-up display and provides an inexpensive and compact alternative to the existing virtual image head-up display systems used in automobiles. The major contribution in this topic has been the analysis of the partially reflective coatings in the index-matched screen. Its effect has been modeled, simulated and a limiting condition on the optical path difference created by the coating for diffraction limited operation has been derived. An alternative screen design based on reflective dual MLA has been introduced and it has been shown that the screen can be used as an alternative to the single MLA screen, offering higher gain and better eyebox uniformity. Although the scheme works well as a reflective screen, for HUD applications, the screen is placed on the dashboard and a ghost image problem limited its use for this application.

One of the major contributions of this thesis has been the patent pending design of the rotated MLA screen. Rotating each microlens in the array such that the chief rays of the incident light are focused on the user's eyes has been the first of its kind in the literature. By concentrating all of the light on the user's eyes, gains on the order of 100 can be achieved. The rotated MLA can be made either as a transparent or an opaque screen. This screen technology has a very promising future in the emerging field of head-mounted projection displays. The design methodology and simulations for the rotated MLA screen have been published in Ref. [23] and a US patent application has been filed.

# 2 SINGLE MICROLENS ARRAY SCREEN

We used reflective MLA based exit pupil expanders in our high gain screen designs because their eyebox size is easily controllable by setting the numerical aperture of the microlenses to the correct value and the fabrication processes of MLAs are well studied. One key advantage of MLAs compared to diffractive optical elements is that the eyebox size is the same for all the wavelengths [20], [21]. As a result, the color balance across the overlapping eyeboxes is very good. Moreover, as the MLA surface is very smooth, the angular expansion is very uniform and there is virtually no speckle on the screen, which is particularly important when using it with laser projectors.

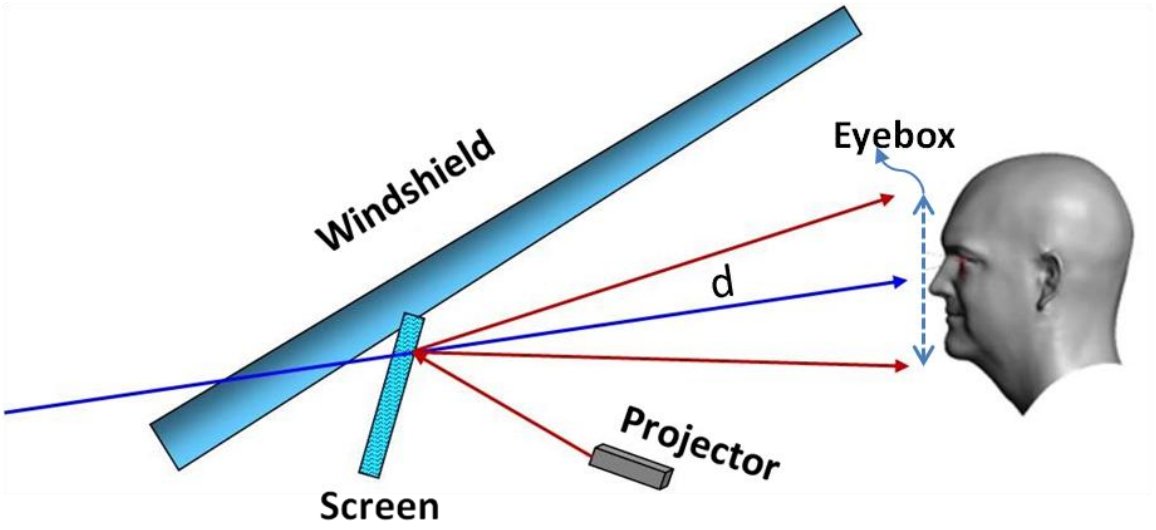


Figure 2.1: The MLA screen in a conceptual drawing for direct projection automotive HUD applications.

## 2.1 Microlens Array Design and Fabrication

### 2.1.1 Optimizing the MLA pitch

As the MLA is a periodic structure it creates diffraction orders when illuminated with coherent light. Setting the correct spacing for the diffraction orders is crucial for creating a uniform eyebox for the user. In our design we assumed that the maximum distance between the user and the screen is 1m and the minimum eye pupil size is 3mm. From these assumptions we can say that the maximum spacing between the diffraction orders corresponding to the longest wavelength of the system should be at most 3mm at the user's position, so that the eye cannot perceive the dark spaces between the diffraction orders.

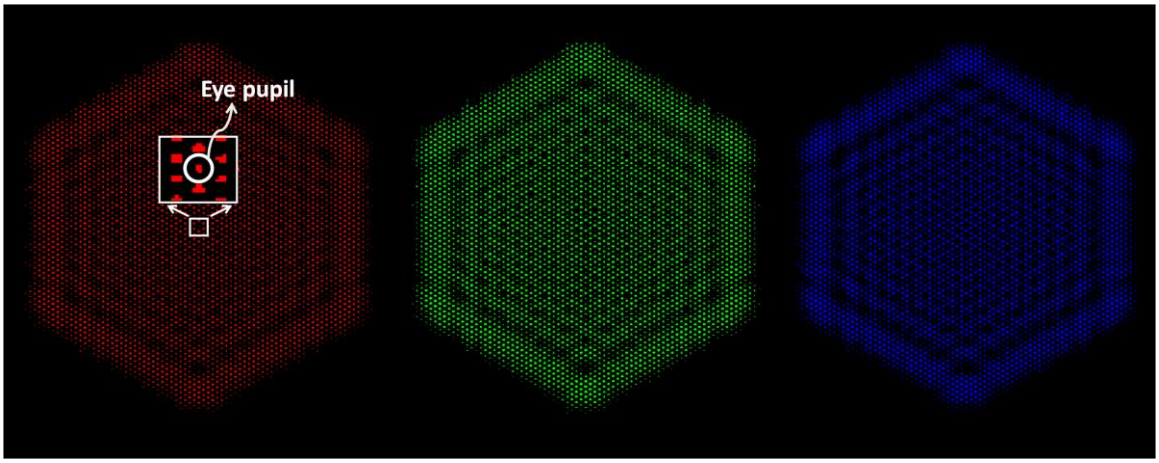


Figure 2.2: Physical optics simulations of a hexagonally packed MLA for RGB wavelengths.

Figure 2.2 shows the simulated eyeboxes of a hexagonally packed MLA for RGB wavelengths of the laser pico-projector we use. MLA creates eyeboxes with the same size that are composed of discrete diffraction orders, as expected. By keeping the diffraction order spacing smaller than the eye pupil, excellent color balance is achieved across the

eyebox. Figure 2.3a shows the combined version of the individual RGB eyeboxes shown in Figure 2.2. The combined eyebox still shows discrete steps between the diffraction orders but as the eye pupil is larger than the diffraction order spacing, it acts as a low-pass filter, smoothing the discrete intensity profile across the eyebox, as shown in Figure 2.3b.

The angular separation between the diffraction orders is governed by Eq.(2-2), where λ is the wavelength and Λ is the MLA pitch [1]. The desired angular separation is given in Eq. (2-2), where p is the minimum pupil size and d is the distance between the screen and the user. As p=3mm and d=1000mm in our case, the maximum angular separation is calculated as 2.99mrad. The longest wavelength of the laser projector we use is 645nm. Plugging in θ=2.99mrad and λ=645nm into Eq. (2-2), the minimum value for the MLA pitch is calculated as 215μm. In our designs we selected the MLA pitch as 300μm.

$$\sin(\theta) = \frac{\lambda}{\Lambda} \tag{2-1}$$

$$\theta = \tan^{-1}\frac{p}{d} \tag{2-2}$$

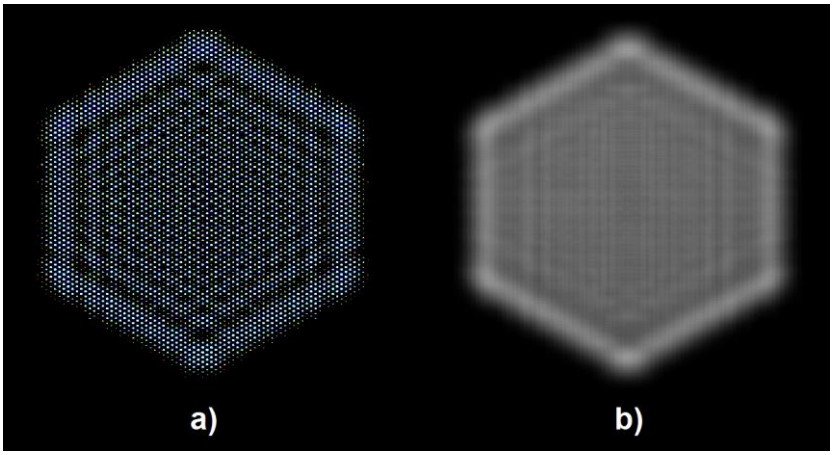


Figure 2.3: On the left the combination of the RGB eyeboxes creating the true color eyebox. On the right, the averaging effect of the eye pupil.

### 2.1.2 Optimizing the microlens curvature

Each microlens expands the incident light with a certain divergence angle based on its aperture size and radius of curvature. The aperture size, or the MLA pitch, is set by the calculations based on diffraction grating theory, as discussed in Chapter 2.1.1. The radius of curvature (R) should be calculated based on the desired eyebox size. Figure 2.4 illustrates the optimization problem. The unit vector from the projector to the top corner of the screen is shown as $\mathbf{V_i}$ in the figure. As the chief ray follows the specular reflection, the reflected unit vector $\mathbf{V_r}$ can be calculated by using Eq.(2-3), where **n** is the surface normal of the screen [26].

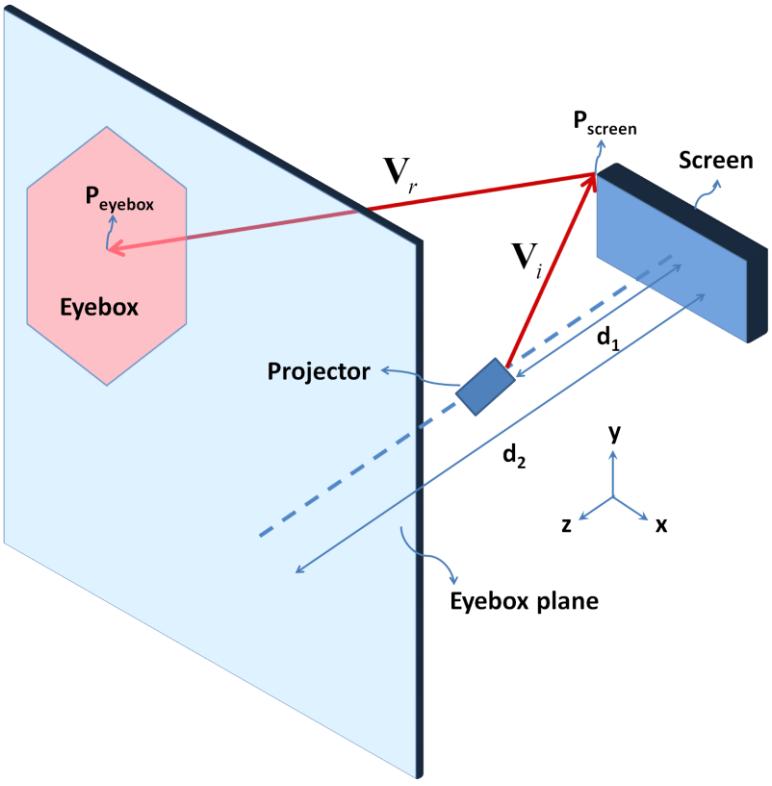


Figure 2.4: Illustration of calculating the center of the marginal eyebox.

$$\mathbf{v}_r = \mathbf{v}_i - 2(\mathbf{v}_i \bullet \mathbf{n})\mathbf{n} \tag{2-3}$$

$$\mathbf{P}_{\mathbf{eyebox}} = \mathbf{P}_{\mathbf{screen}} + \frac{d_2}{\mathbf{v}_\mathbf{r} \bullet \mathbf{n}} \mathbf{v}_\mathbf{r} \tag{2-4}$$

The center of the eyebox can be calculated using Eq.(2-4), where $\mathbf{P}_{\mathbf{screen}}$ is the vector defining the coordinate of the top corner of the screen, $\mathbf{P}_{\mathbf{eyebox}}$ is the coordinate of the center of the eyebox corresponding to $\mathbf{P}_{\mathbf{screen}}$ and $d_2$ is the distance between the eyebox plane and the screen. The symmetric point of the $\mathbf{P}_{\mathbf{eyebox}}$ with respect to the y-axis, $\mathbf{P'}_{\mathbf{eyebox}}$, should be calculated and the size of the eyebox should be selected such that their overlapping region meets the desired eyebox size as illustrated in Figure 2.5.

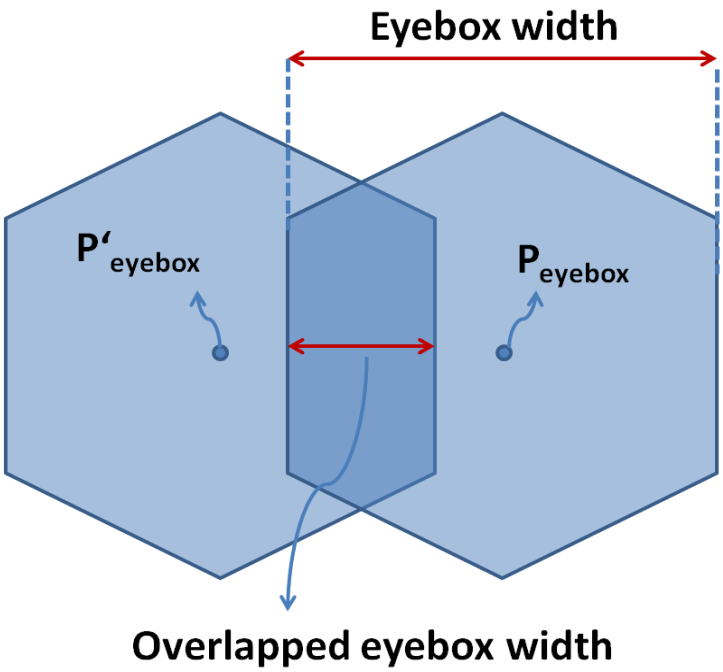


Figure 2.5: The individual eyebox size should be selected such that their overlapped region has the desired eyebox size width.

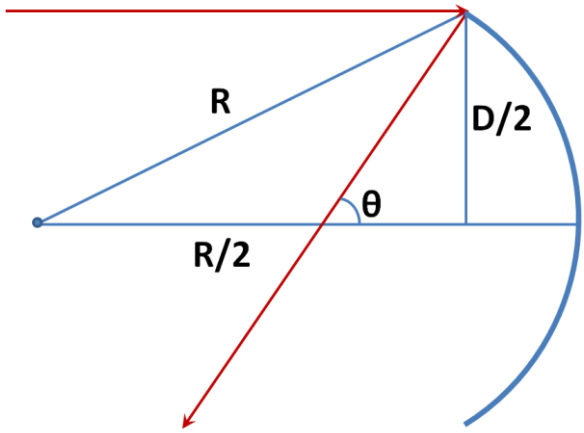


Figure 2.6: The radius of curvature of the microlenses can be calculated using the MLA pitch and divergence angle.

With the calculated MLA pitch in Section 2.1.1 the radius of curvature of the microlenses should be calculated such that the individual eyebox size meets the desired size as discussed above. Eq.(2-5) gives the required half divergence angle (θ) that is shown in Figure 2.6, to achieve the eyebox size in terms of half eyebox width (x) and screen to user distance (d). Eq. (2-6) gives the radius of curvature in terms of the half divergence angle (θ) and half MLA pitch (D/2) such that the incident beam is expanded to meet the desired eyebox size.

$$\theta = \tan^{-1}\left(\frac{x}{d}\right) \tag{2-5}$$

$$R = \frac{D}{3\sin\theta}\left(\sqrt{\cos^2\theta + 3} - \cos\theta\right) \tag{2-6}$$

### 2.1.3 Microlens Array Fabrication

Fabrication of microlens arrays has been well studied in the literature and there are many different fabrication technologies [13]. Grayscale lithography and photoresist reflow

techniques can be given as examples [14][15][16][17]. In our studies the designed MLA screens were fabricated by Microvision Inc, USA and their exact fabrication process is confidential. The preferred method is the isotropic etching of quartz substrate, similar to the method described in [18]. Once the master mold is fabricated, many MLA screens can be made using epoxy casting.

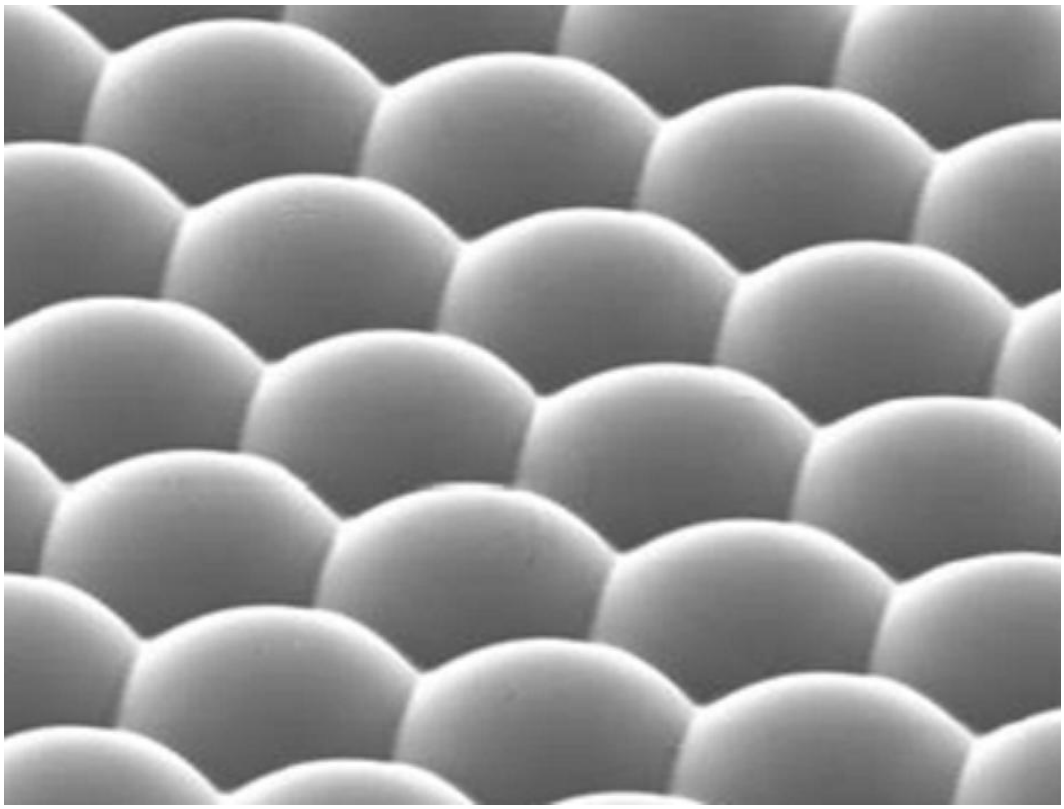

Figure 2.7: A hexagonally packed microlens array.

## 2.2 Transparent Augmented Reality Screen

### 2.2.1 See-through screen principle

The partially reflective coated MLA can be turned into a transparent augmented reality screen by burying the microlenses between refractive index matched layers of any transparent material, as illustrated in Figure 2.8. As a result, the transmitted light sees a phase object with negligible phase variation across the MLAs, whereas the reflected light gets expanded by the MLA and creates an eyebox for the viewer. In other words, for the reflected light the screen behaves like a bright screen with a limited viewing window and for the transmitted light it behaves essentially like an ordinary glass. Although the whole structure is index matched, the thickness of the partially-reflective coating introduces some phase function to the transmitted light, whose effect is discussed in Chapter 2.2.2.

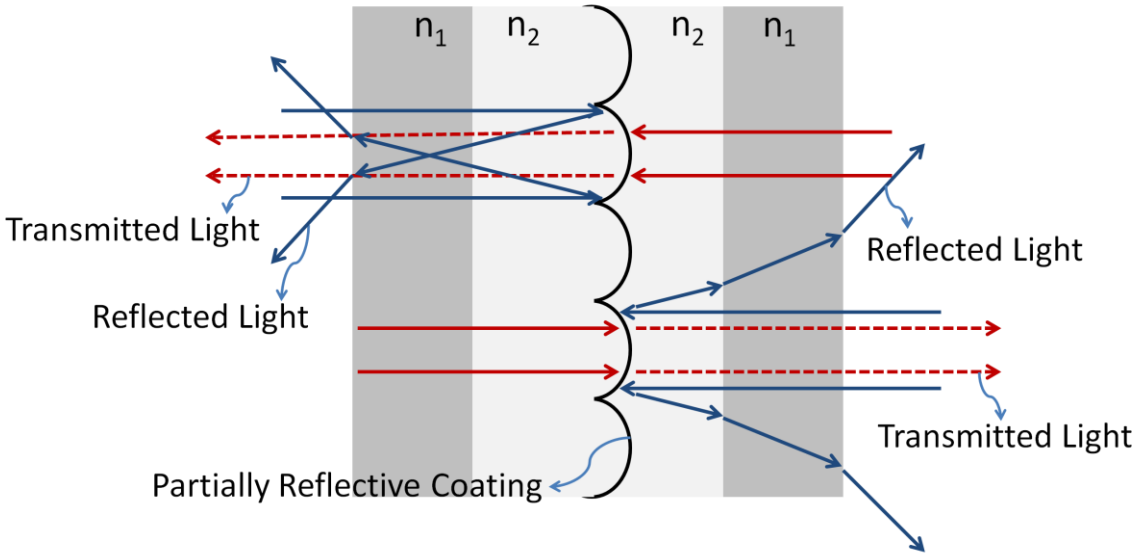


Figure 2.8: The transparent augmented reality screen structure.

The screen can be manufactured in many different ways for different applications. In direct projection automotive HUDs the embedded see-through screen structure can substitute the PVB (PolyVinyl Butyral) layer that is typically sandwiched between the two glass layers of the windshield to create safety glass. It can be embedded into window glasses where necessary or it can be made into a portable piece of glass as shown in Figure 2.18 and Figure 2.19. The see-through screen itself is a sandwich structure beginning with a molded MLA that has the desired form of rotated microlenses. The MLA is then coated with a partially reflective thin coating. Either metal or dielectric partial-reflective coatings could be used depending on the desired properties of the screen. Finally, the coated surface is covered with another layer of the same material used under the coating layer so that the partially reflective coating is the only index mismatch in the full sandwich structure. The whole structure is buried between the layers of some protective cover glasses.

Since the screen has a symmetrical structure it can be used from both sides simultaneously. The only difference is the curvature of the microlenses, i.e. for one side it is concave and for the other side it is convex. This difference does not have an impact on the screen operation because for the concave side the image is formed less than 1mm in front of the screen and for the convex side the image is formed less than 1mm behind the screen. The different image locations cannot be perceived by the human eye. The crosstalk between the two sides of the screen when used by two people, as in Figure 2.19, has been measured by projecting a white page from one side only. The luminance both on the projected side and the back side are measured. The average luminance on the back side is divided by the average luminance on the projected side to find the cross-talk ratio. The experiment was also repeated for the other side. The crosstalk is measured to be less than 1.3% as shown in Table 2.1.

Table 2.1: The luminance values for the crosstalk measurements.

| | Average Luminance on Side #1 ($cd/m^2$) | Average Luminance on Side #2 ($cd/m^2$) | Crosstalk (%) |
|---|---|---|---|
| Projection on Side #1 | 353.021 | 4.251 | 1.20 |
| Projection on Side #2 | 4.800 | 374.589 | 1.28 |

The screen has a gain of about 3 compared to a Lambertian scatterer. The gain is calculated using Zemax simulations where a 100% reflective Lambertian scatterer and 100% reflective MLA screen are compared. The average intensity in the overlapped eyebox for the MLA screen is divided by the average intensity for the Lambertian scatterer to calculate the gain. By rotating the microlenses towards the user, we can improve the efficiency of the screen substantially and can offer brightness gains on the order of 100, as discussed in Section 4.

### 2.2.2 Impact of reflective coating on the screen transparency

Many choices are available for the partially reflective coating. We have tried thin metal coating and two different designs for wavelength selective notch coatings as the reflector layer on the MLA. A single layer metal coating is the simplest for our demonstrators. The thickness of the metal controls the reflectance of the screen and in our experiments: 40Å aluminum coating resulted in average values across the visible band of about 35% reflectance and 50% transmittance, and 15% absorption [1]. With metal coatings there is a trade-off between the transmittance and the reflectance, so the thickness of the coating should be optimized for specific applications. A thin metal coating is a good choice for

broadband sources like LED based projectors. If a laser projector is used, more advanced coatings are possible, such as a notch coating that reflects nearly 100% of the RGB laser wavelengths and transmits nearly 100% of the visible spectrum outside of the reflective notches. We designed the notch coating shown in Figure 2.9 for a laser pico-projector that has the RGB wavelengths of 645nm, 532nm and 445nm.

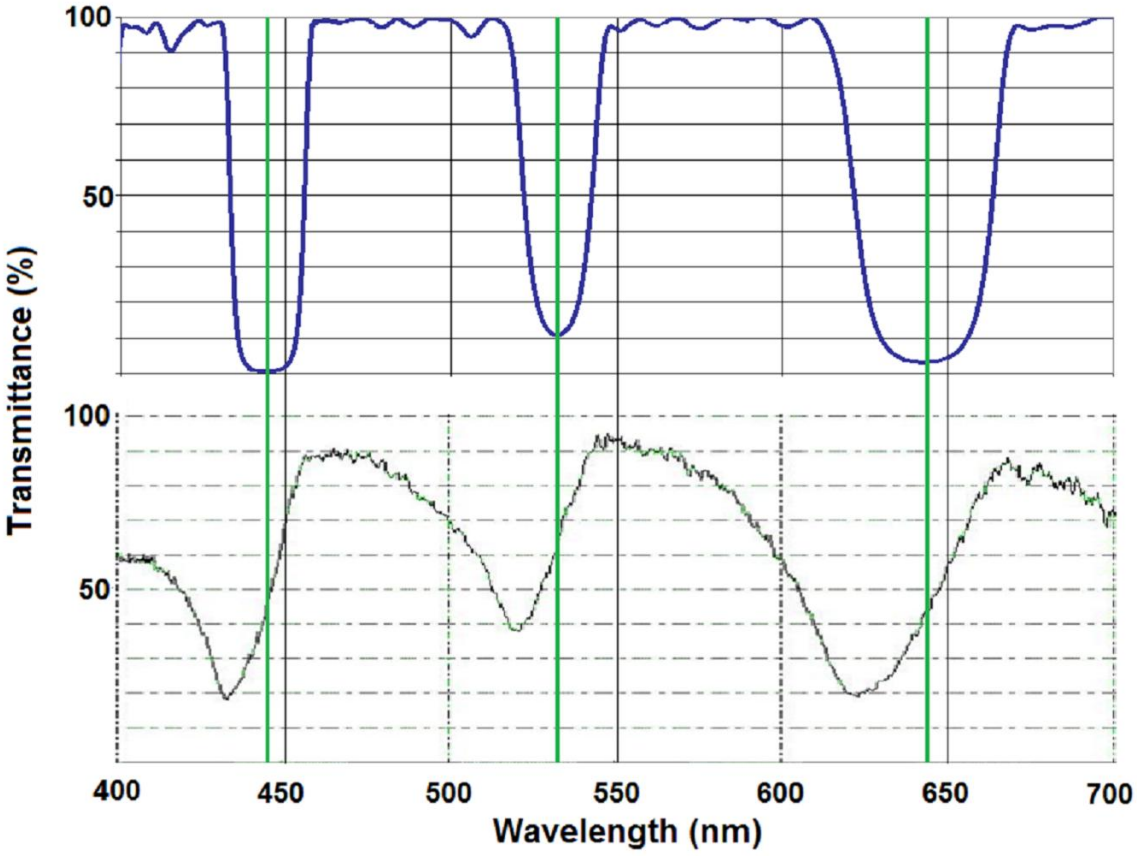


Figure 2.9: Specifications of the designed notch coating on top, measured characteristics of the fabricated coating at the bottom.

The transmission bands of the fabricated screen was measured with a grating spectrometer and found to be shifted from the original coating specifications as seen in

Figure 2.9. This resulted in some error in the transmittance and reflectance values and the coloration of the screen. Figure 2.10a shows the imaging setup to test the coated screens. While the metal coated screen appears in the correct color, the notch coated screen has a pinkish hue, which is primarily due to the measured transmittance characteristics in Figure 2.9. Improving the coating process can in principle eliminate this problem. While the metal coated screen produces a sharp image, the notch-coated screen degrades the resolution as seen in Figure 2.10b. The blurring effect is quantified by measuring the MTF of the screens as discussed below.

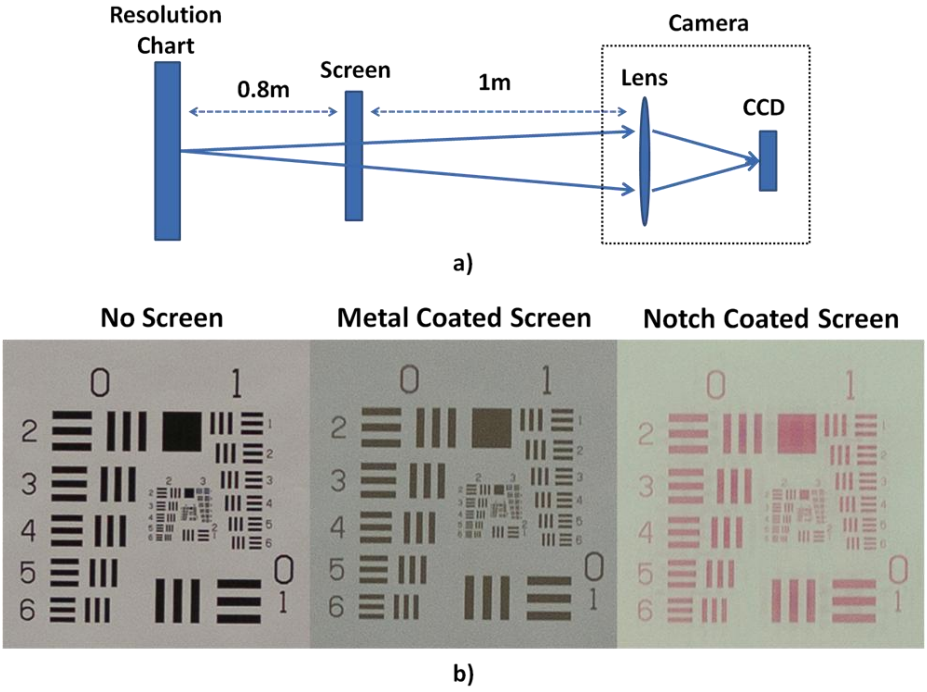


Figure 2.10: a) The experimental setup of the resolution measurements. b) The captured images of the resolution chart through the screens.

With the index matched screen structure that was shown in Figure 2.8, the screen should not have any effect on the transmitted light. However, as seen from the MTF

curves, thick coatings can degrade the resolution. Since the notch coating is thick, it introduces some phase function across each microlens and as the MLA structure is periodic, the phase function results in diffraction orders. To test the presence of diffraction orders emanating from the screen, the screen was illuminated with a 3mm collimated beam from a laser diode. The diffraction orders are faint compared to the central spot and only visible when the logarithm of the image intensity is displayed as seen in Figure 2.11a. Since MLAs are packed in a hexagonal fashion, there are six $1^{st}$ order diffraction spots surrounding the central $0^{th}$ order. Figure 2.11b shows the physical optics simulations for the same scenario. The details in between the diffraction orders observed in logarithmic scale in Figure 2.11b are mostly due to interference and are missing in Figure 2.11a due to the limited dynamic range of the camera. To quantify the noise due to diffraction and scattering, the encircled intensity plot of the experimental PSF is calculated as shown is Figure 2.11c, which is the integral of the intensity inside a circle with an increasing radius. If the phase variations due to the partially reflective coating were negligible and there were no noise due to scattering and diffraction, we would expect to see a step function with a smooth transition from zero to one. In the real case we have diffraction orders due to the coating thickness, thus we observe two steps in the encircled intensity plot. The variations between those steps are mainly due to diffraction and scattering noise.

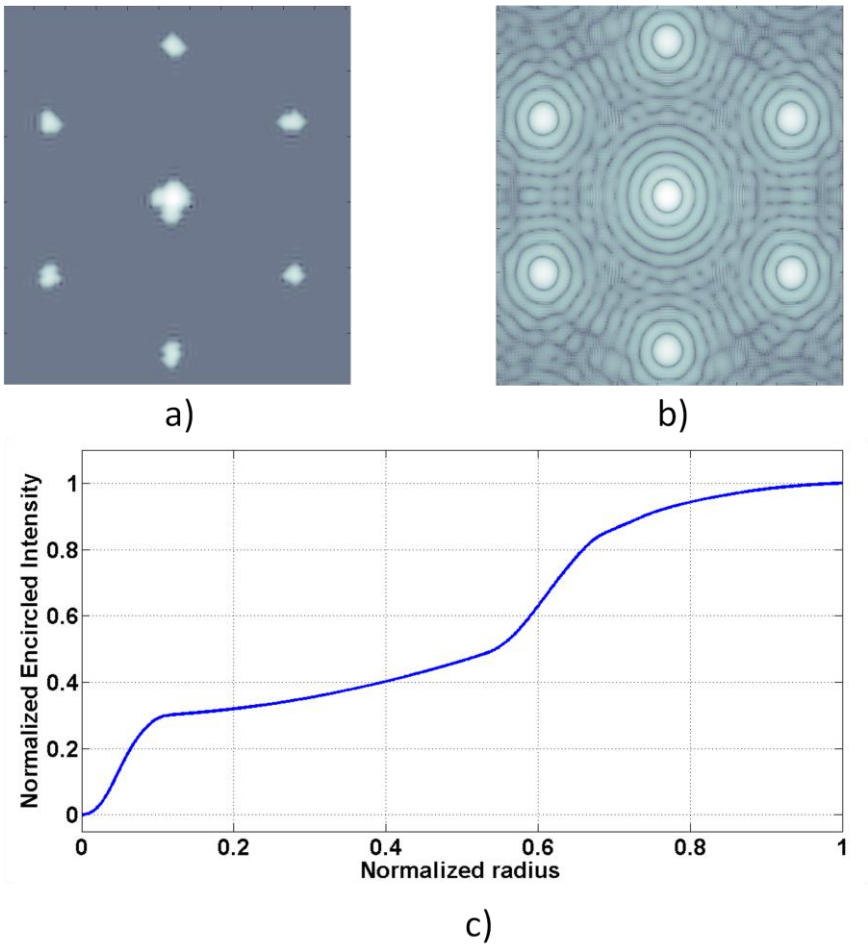


Figure 2.11: a) Experimental PSF of the system. b) Simulated PSF of the system. c) The encircled energy plot of the experimental PSF.

We used the slanted edge technique to measure the MTF of the MLA screens [6]. An experimental setup similar to Figure 2.10a was used, where the resolution chart was replaced by an LCD computer monitor. A slanted edge with a 5° angle was displayed on the LCD located 80cm from the MLA screen, followed by a CCD camera at 1m distance to the MLA screen. Figure 2.12a shows the slanted edge image on the camera. First the

Canny edge detection algorithm is applied to find the edge [7]. The angle of the slanted edge is subsequently computed using Principal Component Analysis (PCA) [8]. The image is up-sampled by a factor of four and the edge is straightened by an affine transformation of the whole image using the computed angle. The resultant image is shown in Figure 2.12b. The average of the columns of Figure 2.12b results in the oversampled edge profile, which is the 1D edge spread function (ESF) of the system, as shown in Figure 2.12c. Figure 2.12d shows the derivative of the ESF, which is the point spread function (PSF) of the system. MTF is obtained by calculating the modulus of the Fourier Transform of the PSF and normalizing the resultant transfer function.

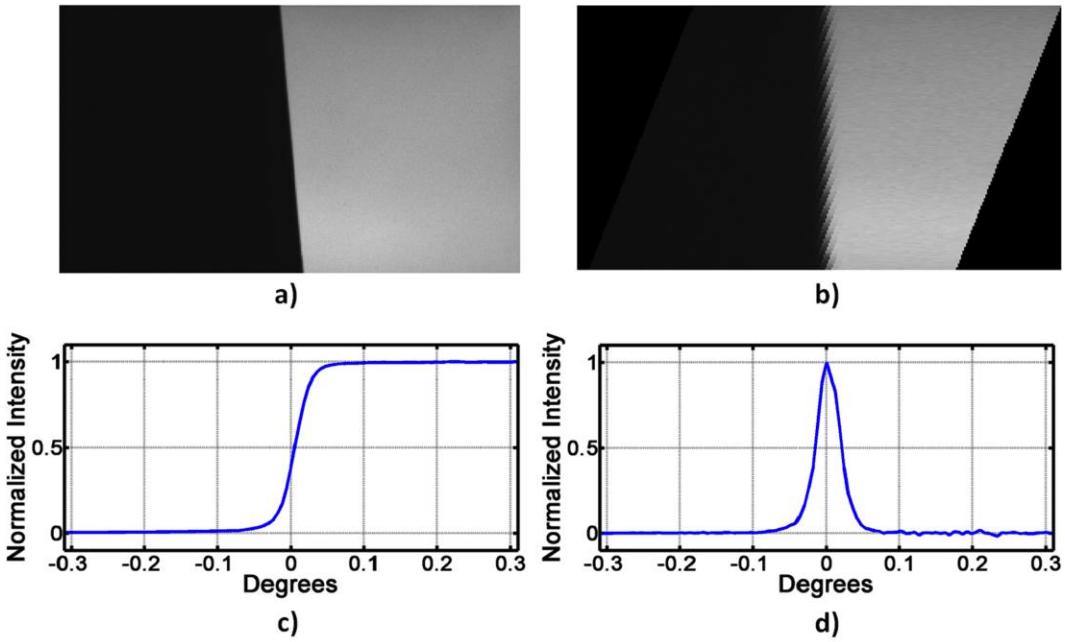


Figure 2.12: Steps of the slanted edge MTF measurement technique.

With the method described above, the MTF curves for the thin metal and notch-coated screens are obtained, as illustrated in Figure 2.13. The free space MTF shows the MTF of

the imaging system without any screen for reference. The camera lens diameter and f/# were adjusted to obtain a cut-off frequency of around 30cyc/deg in the experiments to make it consistent with the performance of the 20/20 vision for human eye. As seen in the figure, the metal coating and the 'no screen' MTF curves match very well, showing that the index-matched structure behaves as expected. For MTF50, that is the MTF falling to 50%, the bandwidth of the notch coated screen is reduced almost by half, compared to the 'no screen' MTF. The reduced bandwidth explains the blurring observed in Figure 2.10.

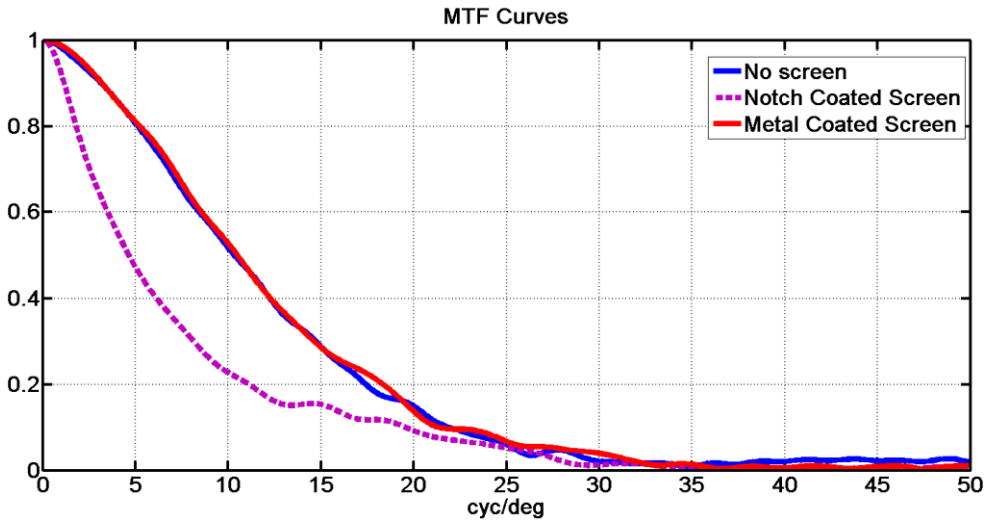


Figure 2.13: Measured MTFs of the screens with different coatings.

The main problem associated with the MTF degradation is due to the thickness of the coating layers. As shown in Figure 2.14a, even though the coating thickness is uniform, the lens curvature introduces an optical path difference (expressed as Δ in Eq.1) between the light transmitted through the center and the edges of the lenses, where p(x,y) is the length of the ray path inside the coating, which varies between *t* and $t_{max}$ from the center to the edge of each microlens. A parametric plot of the Δ created by the coating is given in Figure 2.14b. The phase function associated with a single microlens is shown in Eq.2 and the

phase function for an array of microlenses can be expressed as in Eq.3, where ** denote 2D convolution and $d_x$ and $d_y$ denote the pitch of the MLAs in each axis.

$$\Delta = \left( p(x,y) - t \right)\left( n_3 - n_2 \right) \tag{1}$$

$$\phi(x,y) = \exp\left( j\frac{2\pi}{\lambda}\Delta \right) \tag{2}$$

$$t(x,y) = \phi(x,y) ** \sum_i \sum_j \delta(x - id_x)\delta(y - jd_y) \tag{3}$$

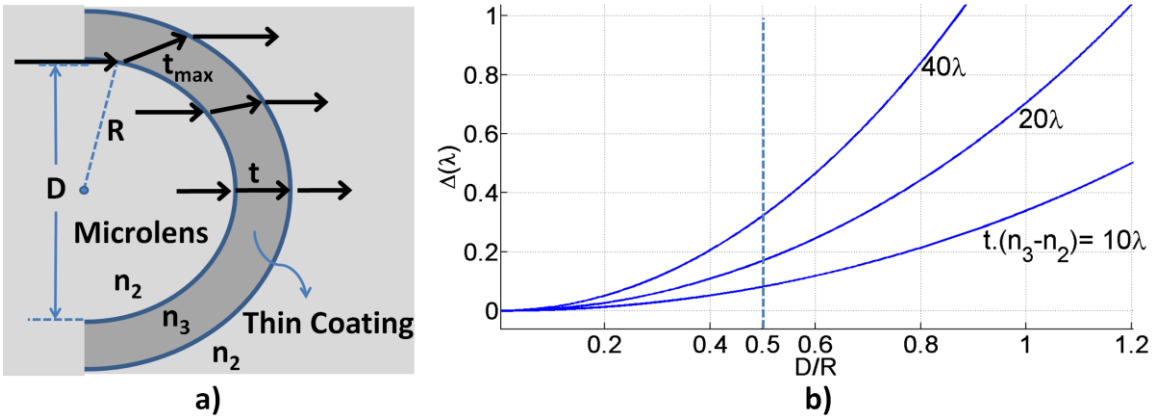


Figure 2.14: a) The path difference created by the coating layer on the MLA. b) The plot of the phase difference as a function of microlens parameters and the coating thickness.

We performed physical optics simulations to see the effect of this phase function using MATLAB [9]. In our code, a 3mm diameter area on the screen is illuminated with a collimated, monochromatic light with λ=550nm. The screen is a hexagonally packed MLA with 300μm pitch, where each hexagon is filled with the phase function exp(j2πΔ/λ), as shown in Figure 2.15. After the light passes through the screen, it propagates 1m and is focused by a lens. The resulting intensity is compared to the diffraction-limited system, i.e. uniform phase function, to find the Strehl ratio of the actual system.

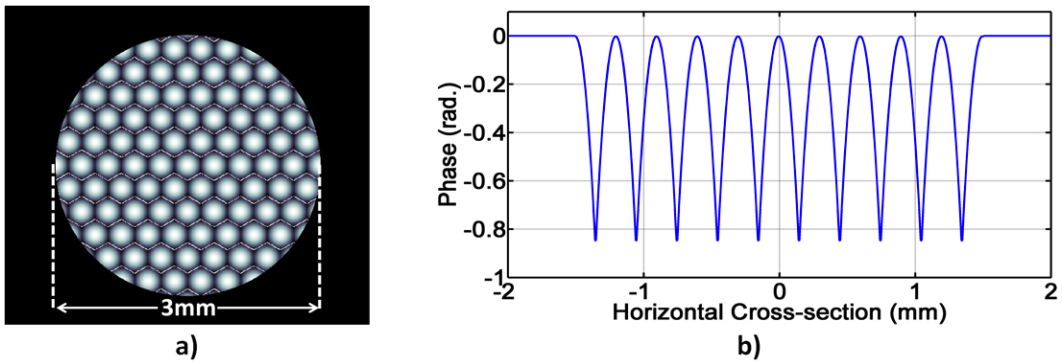


Figure 2.15: a) The phase of the simulated portion of the MLA. b) The horizontal cross-section of the phase function.

We simulated three different cases to see the relationship between the $\Delta$ and the Strehl ratio, as seen in Figure 2.16. In each subsection Figure 2.16 the real part of the phase function $\exp(j2\pi\Delta/\lambda)$ is shown on the left and the Strehl ratio for the corresponding $\Delta$ is shown on the right. In Figure 2.16a the Strehl ratio is 0,91 and the real part of the phase function is non-negative. In Figure 2.16b the Strehl ratio is 0,79 and the real part of the phase function starts to show negative values at the corners of the hexagon. In Figure 2.16c the Strehl ratio is 0,31 and the negative values gets more dominating in the real part of the phase function. It is generally assumed that the human eye can differentiate the aberration effects for Strehl ratios less than 0,8 [10]. From the simulations we conclude that the real part of the phase function should be greater than zero to satisfy this condition. This means $\cos(2\pi\Delta/\lambda) \geq 0$, so $\Delta \leq \lambda/4$ to eliminate aberration artifacts introduced by the coating. This is essentially identical to the well known Rayleigh criteria. The metal-coated screen has a film thickness of about 40Å and a refractive index of about 1.09 in the visible band [11], which creates a peak-to-valley OPD of $0.0006\lambda$ and results in a Strehl ratio of 0.998. However, the notch coating has more than hundred layers of coatings with refractive index of about 2,5 to 3 for some coating layers, which violates the condition $\Delta \leq \lambda/4$.

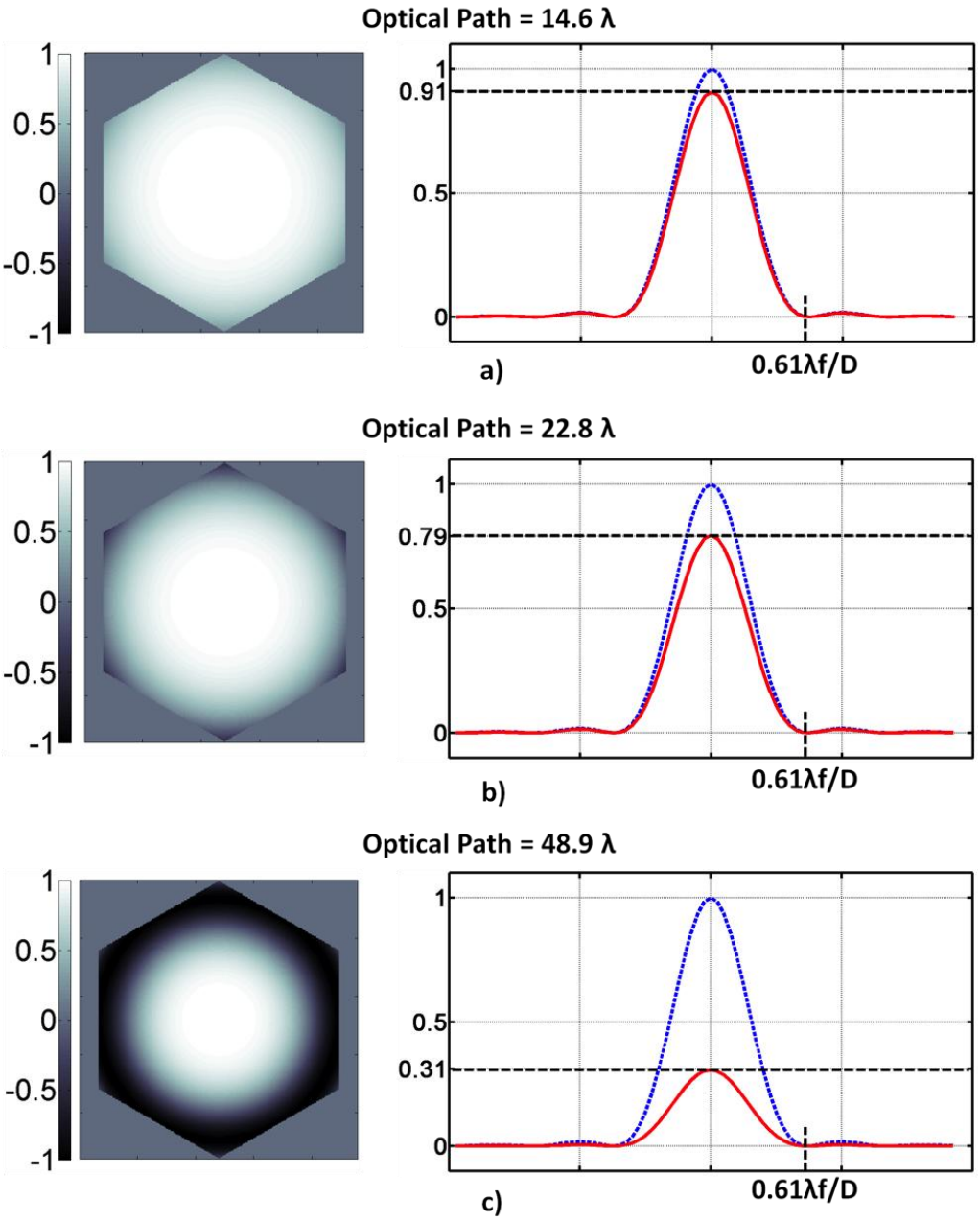


Figure 2.16: The imaginary parts of the phase functions for different coating thicknesses the left, the corresponding Strehl ratios on the right.

## 2.3 Ray optics simulation results

The screen with the parameters above has been modeled and simulated using Zemax software. The radius of curvature of the microlenses is set at 625um, which is optimized using Zemax to yield the desired eyebox size of about 65cm at the user's position. As illustrated in Figure 2.17, a total of 50 equidistant sample points were chosen on 5 equidistant rows across the screen of size 87.5mm x 175mm. The screen size is based on what is currently available for the experiments. The model represents using a scanned laser projector to illuminate the MLA screen. Each incident beam results in a hexagonal eyebox at the driver's position. The eyeboxes shift laterally as the scan angle increases. The sum of eyeboxes in all their shifted positions for the 50 points in the Zemax model can be seen in Figure 2.17. The bright white region at the center of the figure shows where all of the individual eyeboxes overlap that is the useable full viewing window, where every point on the screen can be seen by the user. The width of the full viewing window is ±18°, which corresponds to about 65cm at the user's position that is 1m away from the screen.

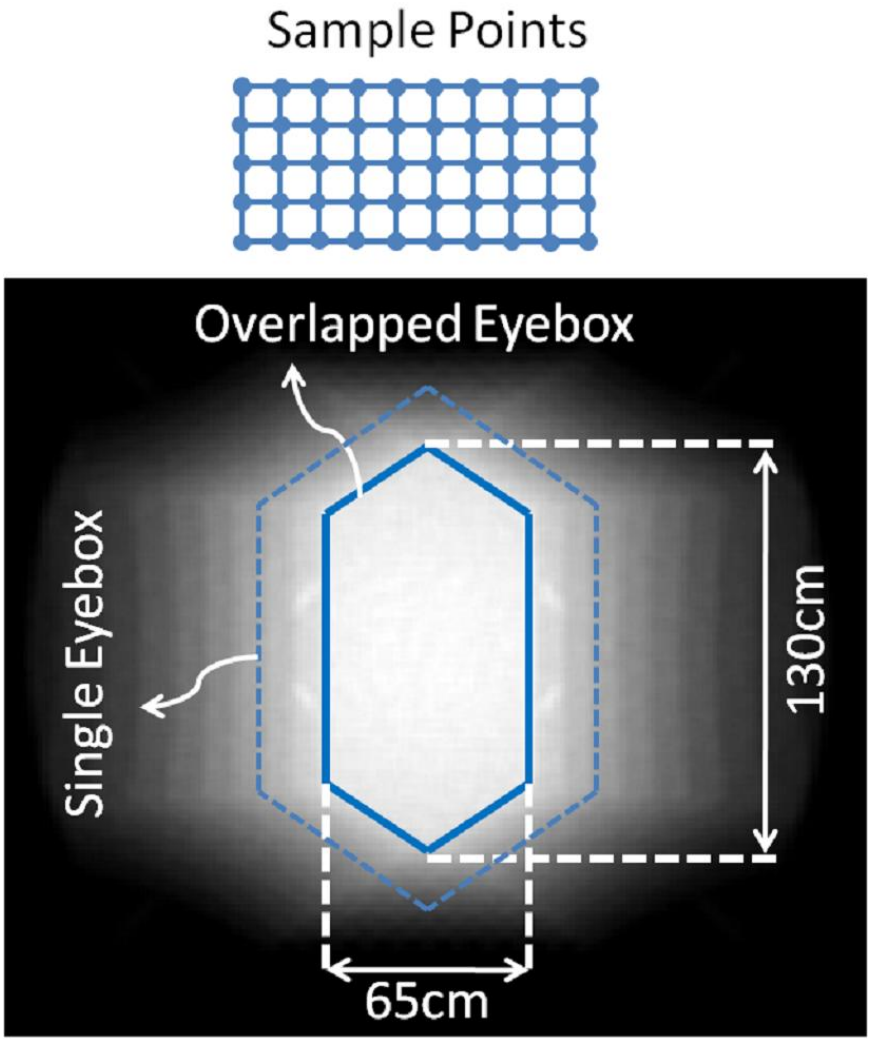


Figure 2.17: The simulated eyeboxes of the sample points on the screen.

## 2.4 Experimental results

We demonstrated that an MLA sandwiched between index matched layers can be used as a see-through screen for automotive HUD applications, as seen in Figure 2.18. The screen was tested in a real car on a real road with a laser pico-projector. It is shown that a

stand-alone transparent MLA screen together with a pico-projector can be used as an automotive HUD, eliminating the need for a large space under the dashboard required for the conventional HUD systems. The MLA creates a bright image with no speckle and good color balance. The wide viewing window of the screen provides a comfortable operating region for the driver. First prototypes were fabricated with two different semi-reflective coatings; a broadband dielectric and a thin metal coating. The HUD demonstrator in Figure 2.18 has broadband dielectric coating with about 15% reflectance.


Figure 2.18: The demonstrator of the automotive direct projection HUD.

The MLA screen is not limited to HUD applications only. It can be used wherever a transparent front projection screen is needed. A useful property of our screen is that it can be projected from two sides at the same time without interference as illustrated in Figure 2.19, provided that the projection angles are set appropriately. It enables new ways of

communication where two people project their personal information onto the same screen, without seeing each other's content but seeing each other through the transparent screen. It may have unique gaming applications.

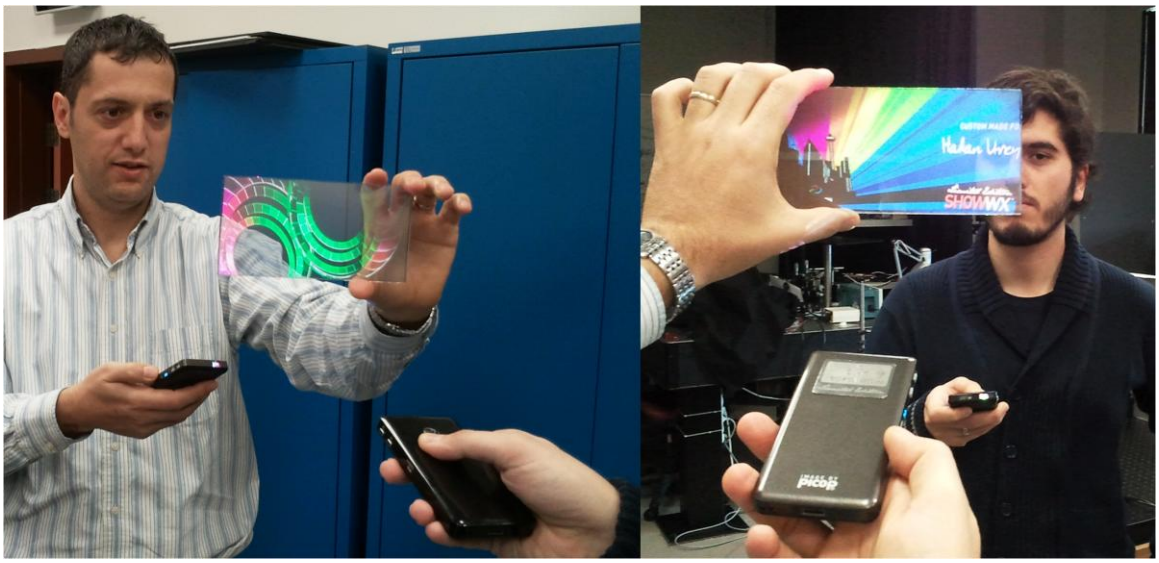

Figure 2.19: Demonstration of the bidirectional operation of the MLA screen.

# 3 DUAL MICROLENS ARRAY SCREEN

## 3.1 Dual MLA screen principle

Dual MLA is a high gain exit pupil expander, which is composed of two identical MLAs that are separated by one focal length of the microlenses. It has two major advantages compared to single MLA exit pupil expanders, which was discussed in Section 2. One of them is the eyebox position for the dual MLA does not change with the changing incidence angle. As a result, the eyeboxes are concentrated in a smaller area; hence the brightness gain is increased compared to a single MLA. The other advantage is that it has superior eyebox uniformity.

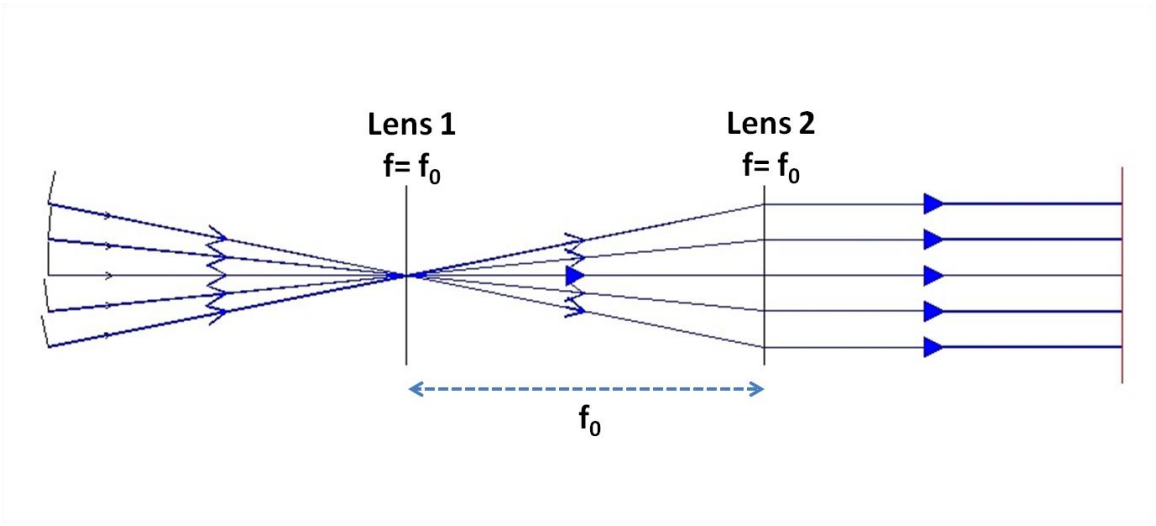


Figure 3.1: The Zemax simulation of the dual MLA, showing the telecentric property of the configuration.

The dual MLA is a telecentric system, meaning that the chief ray of the input light becomes parallel to the main optical axis at the output. The chief ray is the ray that passes through the center of the aperture stop and the aperture stop is the physical opening that

limits the number of rays entering the system [12]. In the dual MLA case the aperture stop is the aperture of the first lens, which is indicated with “Lens 1” in Figure 3.1. The rays passing through the center of the first lens are the chief rays in the system. Since the center of the first lens is exactly located at the focal point of the second lens, the chief rays become parallel to the main optical axis after passing through the second lens, as shown in the Zemax simulation in Figure 3.1.

Unlike the single MLA that was discussed in Section 2, the central direction for the eyeboxes do not follow the usual law of reflection (i.e. angle of incidence equals angle of reflection), due to the telecentricity of the dual MLA. The central directions of the eyeboxes are parallel to the surface normal of the screen, regardless of the incidence angle. As the eyeboxes are expanded around the chief rays by the microlenses, the resulting eyeboxes from the dual MLA are concentrated in a much smaller area, thus the gain of the screen is increased.

The dual MLA is not compatible with our see-through screen that was discussed in Section 2.2.1, because the diffuser layer in the see-through screen structure should consist of a single reflective layer and the thickness of the index mismatch should be negligible. A reflective version of the dual MLA screen can be made by fabricating a single MLA on top of a mirror, placed half the focal length of microlenses above the mirror, as seen in Figure 3.2. This way the light passes through the top MLA layer twice and the distance traveled in between would be exactly one focal length of the microlenses. This technique eliminates the difficult alignment issues encountered in the transmission mode screens.

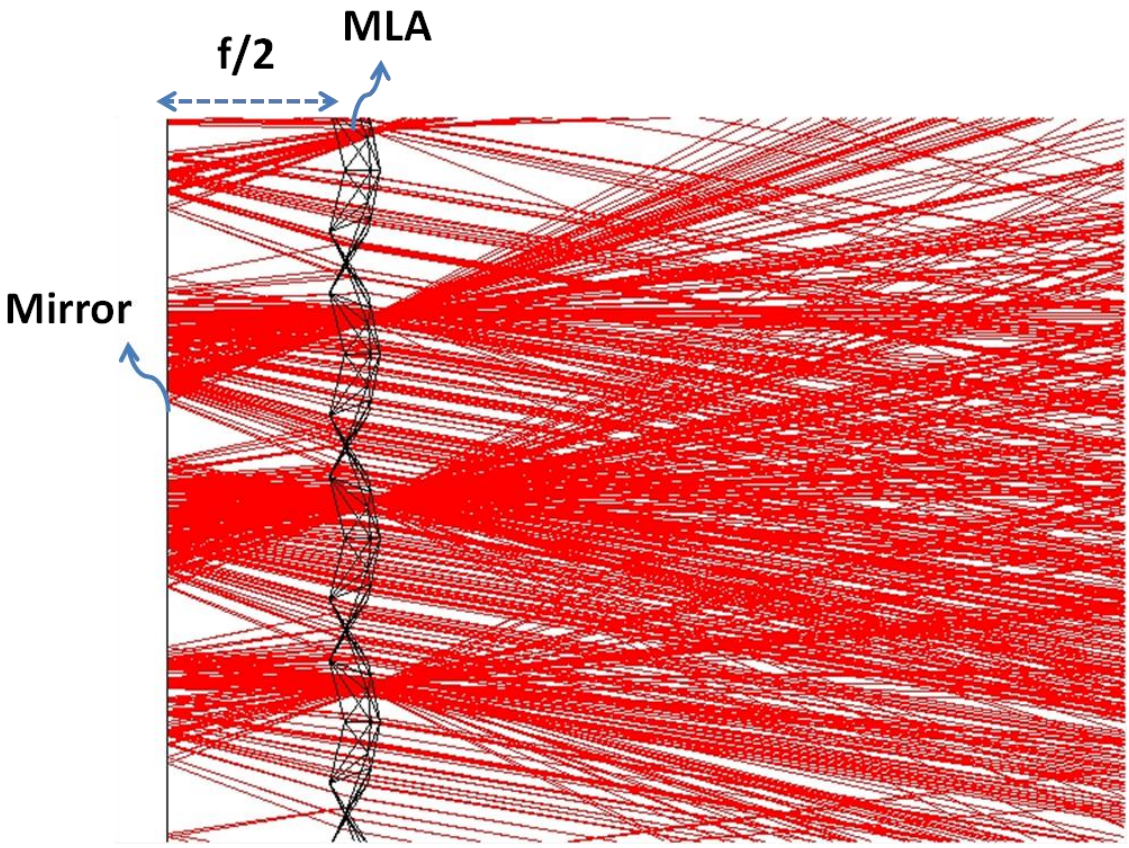


Figure 3.2: The Zemax simulation layout for the reflective dual MLA screen.

Besides the increased gain due to telecentricity, the dual MLA screen has better eyebox uniformity compared to the single MLA screen. This is because the dual MLA creates a perfect optical Fourier Transformer [20]. Eq. (3-1) is the Fresnel diffraction integral where $(\xi, \eta)$ and $(x, y)$ denote the input and output coordinate systems, respectively [1]. The simulation scheme is as follows: the input electric field is multiplied with the transmission function of the MLA in Eq. (3-2) where $aper(\xi, \eta)$ is the lens aperture function. The resulting field is propagated one focal length using Eq. (3-1) and then multiplied with the same MLA once more.

$$U(x,y)=\frac{\exp(jkz)}{j\lambda z}\exp\left(\frac{jk(x^2+y^2)}{2z}\right)\int_{-\infty}^{\infty}\int_{-\infty}^{\infty}\left\{U_0(\xi,\eta)\exp\left(\frac{jk(\xi^2+\eta^2)}{2z}\right)\right\}\exp\left(\frac{-jk(x\xi+y\eta)}{z}\right)d\xi d\eta \tag{3-1}$$

$$t_{MLA}(\xi,\eta)=aper(\xi,\eta)\exp\left(\frac{-jk(\xi^2+\eta^2)}{2f}\right)**\sum_{n=-\infty}^{\infty}\sum_{m=-\infty}^{\infty}\delta(\xi-nd_x,\eta-md_y) \tag{3-2}$$

If the microlenses in the MLA are indexed in a matrix form with indices (i, j), the illumination function for each microlens can be expressed in its own coordinate system as in Eq. (3-3). Each pass through the microlens introduces a quadratic phase function. In the first pass, the quadratic phase function inside the Fresnel diffraction integral is cancelled. In the second pass the phase function outside the integral is cancelled. As a result the beam propagation through the dual MLA becomes a periodic extension of the perfect optical Fourier Transforms of the illumination function $p_{i,j}(\xi,\eta)$ with some constant scaling as in Eq. (3-4).

$$p_{i,j}(\xi,\eta)=I(\xi-id_x,\eta-jd_y)aper(\xi,\eta) \tag{3-3}$$

$$t_{MLA2}(x,y)=\frac{\exp(jkz)}{j\lambda z}\sum_n\sum_m FT\left[p_{n,m}(\xi,\eta)\right]_{\substack{\xi=x/\lambda f\\ \eta=y/\lambda f}}**\delta(x-nd_x,y-md_y) \tag{3-4}$$

## 3.2 Physical optics simulation results

Both the single and the dual MLA screens were simulated using physical optics propagation techniques to assess their eyebox uniformity [9]. As discussed in Section 3.1, the second pass through the MLA cancels the quadratic phase function outside the Fresnel diffraction integral, that's why the dual MLA forms the perfect optical Fourier Transform of the illumination function. Consequently the eyebox uniformity for the dual MLA screen is superior compared to the single MLA.

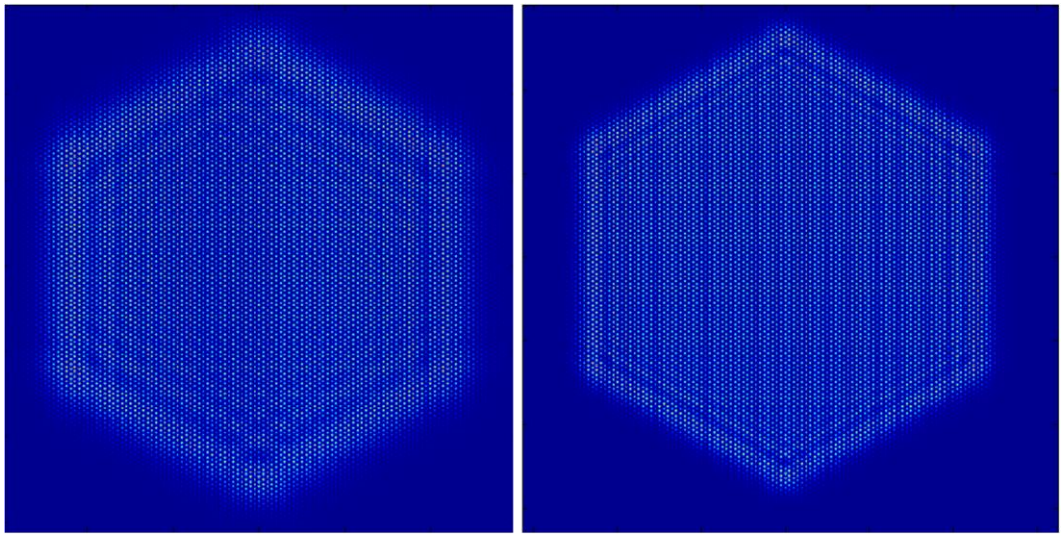


Figure 3.3: Physical optics simulations of the eyeboxes for different MLA screens: Single MLA on the left, dual MLA on the right.

Figure 3.3a and b are the simulated eyeboxes of the single MLA screen and the dual MLA screen, respectively. The eyebox corresponding to the single MLA screen has many ripples, which is very disturbing to the user, especially if the projected image has a background color. The dual MLA eyebox is much uniform except for the edges. Although

the dual MLA is the perfect Fourier Transformer the ripples at the edges are due to the windowing effect of the microlens aperture and the illumination function [22]. The dual MLA is band-limited due to the finite f/# of the microlenses. The horizontal cross-sections of the eyeboxes in Figure 3.3 are shown in Figure 3.4. Unlike the single MLA, the center of the dual MLA eyebox is very smooth, as seen in the figure, so the viewer sees a very uniform image.

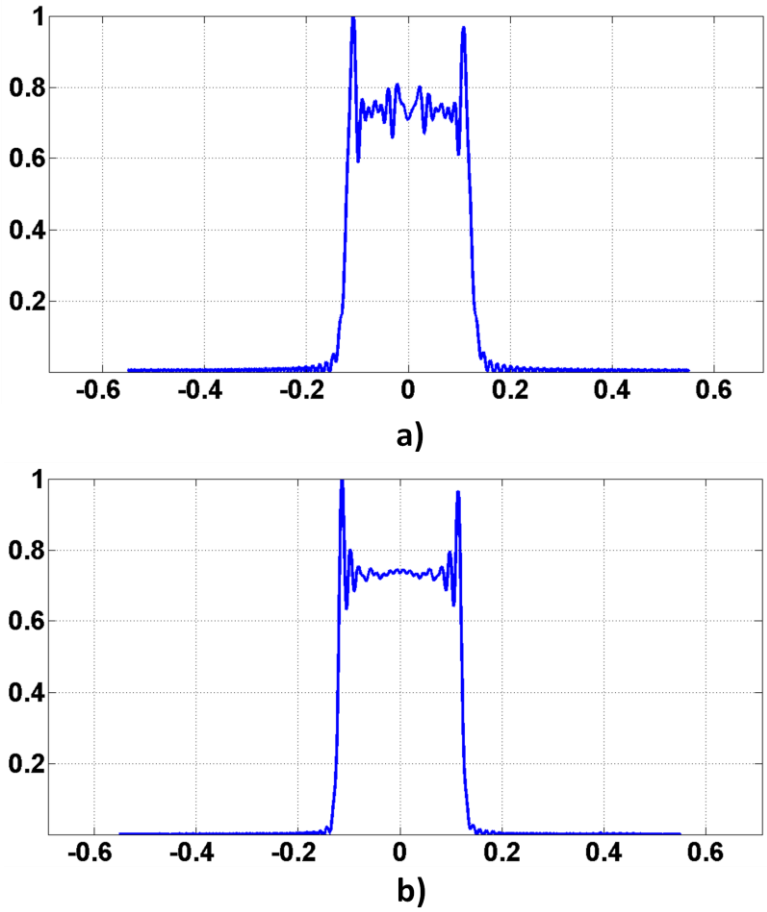


Figure 3.4: The horizontal cross-sections of the eyeboxes in Figure 3.3: Single MLA on top, dual MLA at the bottom.

### 3.3 Ray optics simulation results

The dual MLA screen was modeled and simulated using Zemax to analyze the telecentric characteristic of the screen. In the Zemax model only the four corners and the center of the screen were simulated. As seen in Figure 3.5, the eyeboxes for the dual MLA screen are much more concentrated compared to the single MLA that was shown in Figure 2.17. As a result the dual MLA screen has a calculated brightness gain of about 9, whereas the single MLA screen had a gain of 3, so the dual MLA is three times brighter than the single MLA for the same overlapped eyebox size. The cross-sections of the simulated eyebox are shown in Figure 3.6.

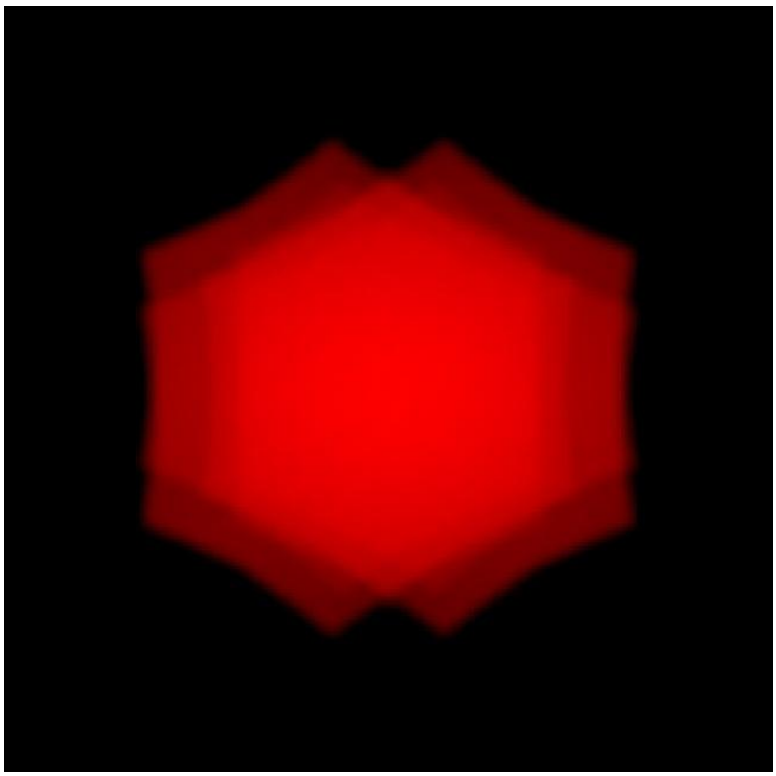

Figure 3.5: The true color detector view of the simulated eyeboxes in Zemax for the reflective dual MLA screen.

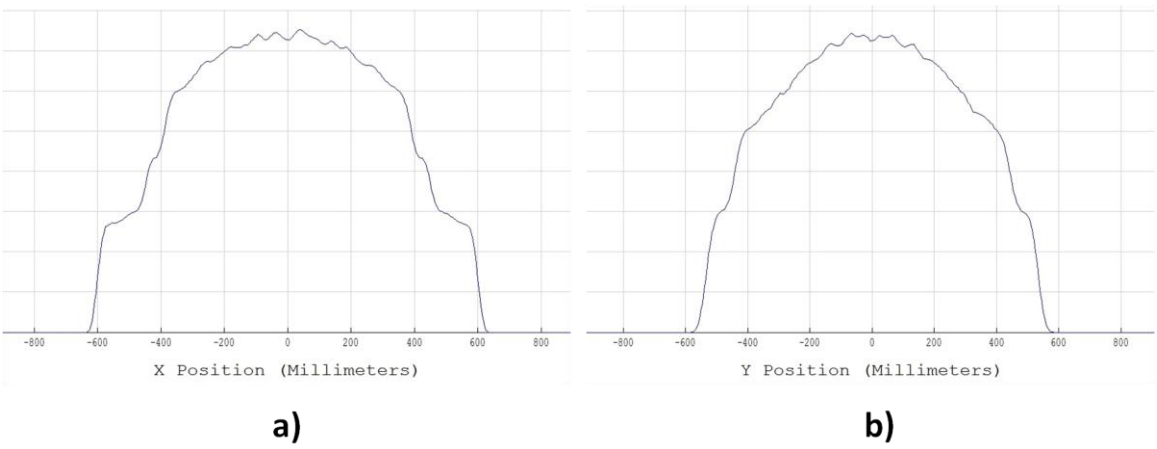


Figure 3.6: a) The horizontal cross-section of the eyebox. b) The vertical cross-section of the eyebox.

## 3.4 Experimental results

The fabricated reflective dual MLA screen was tested as a direct projection HUD screen. The screen is directly projected from the rear-view mirror position and the reflected light from the screen is reflected from the windshield, reaching the driver's eyes as illustrated in Figure 3.7.

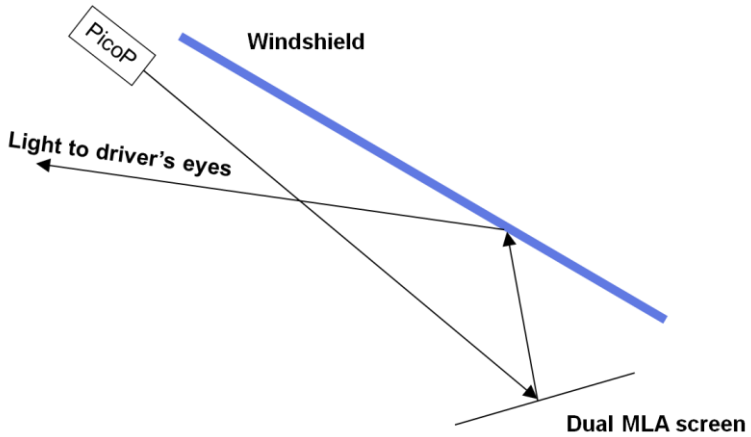


Figure 3.7: The automotive HUD configuration for the dual MLA screen.

As the reflected chief ray follows the surface normal of the screen, the screen is rotated such that its normal is pointing the natural input direction of the windshield such that the reflected light from the windshield reaches the driver. Although the screen works very well as a bright display, the HUD configuration was not very successful. The reason is the image on the dual MLA screen was so bright and it was visible from the driver's position, so two images would be seen by the driver and cause confusion as seen in Figure 3.8.

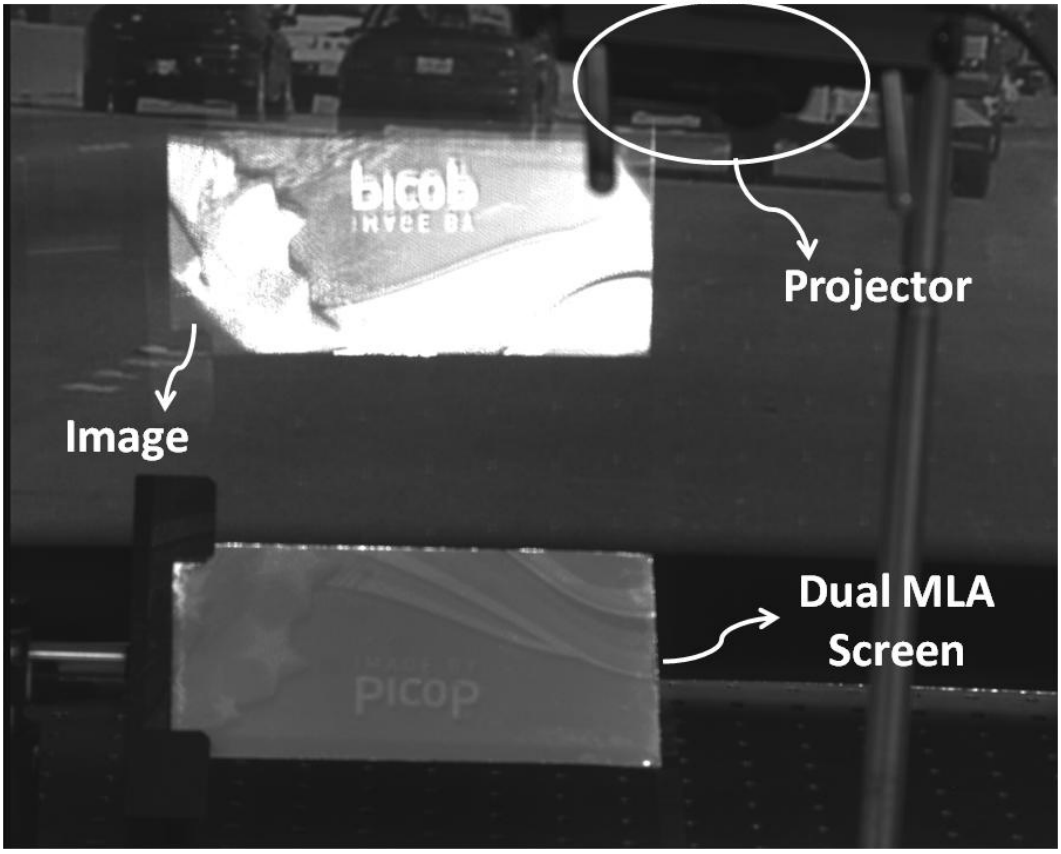


Figure 3.8: The reflective dual MLA screen in the direct projection automotive HUD configuration.

# 4 ROTATED MICROLENS ARRAY SCREEN

The ultimate solution for a high brightness gain display is to have the eyeboxes of every pixel on the screen overlap perfectly at the user's position. Our solution for achieving perfectly overlapped eyeboxes is to rotate each microlens in the screen about two axes by different amounts, such that the chief ray reflected from each microlens is steered towards the user as illustrated in Figure 4.1. As the curvature of the microlenses, which is the same for every microlens, expand the reflected light uniformly, the eyeboxes for every pixel are created around a single target point. Thus, the eyeboxes overlap perfectly and the wasted power at the unused edges of the eyebox is avoided. Limiting the expansion of the eyeboxes by increasing the numerical aperture of the microlenses makes it possible to achieve brightness gains on the order of 100s.

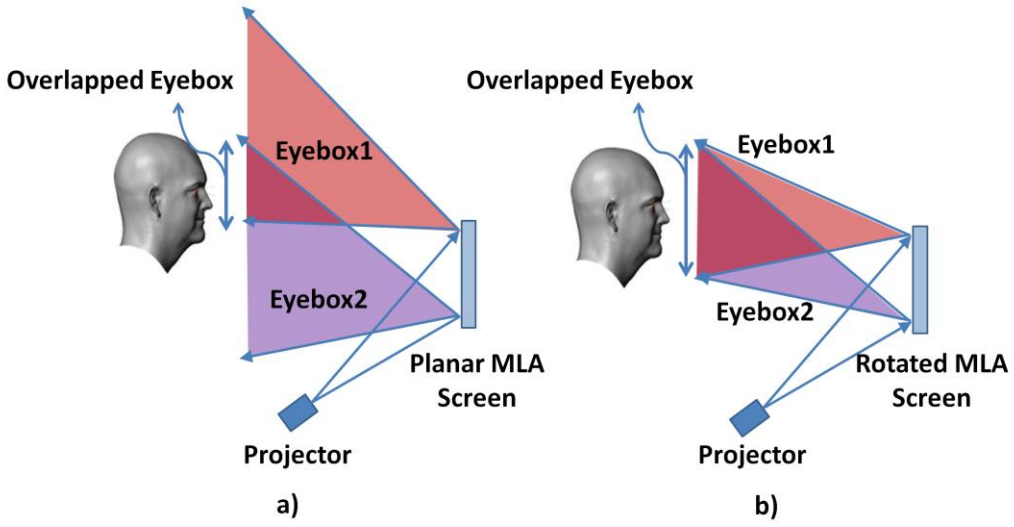


Figure 4.1: The gain of the screen increases with decreasing overlapped eyebox size.

We developed the necessary algorithms to design such a high efficiency screen (transparent or opaque) for any given arbitrary geometry. The design problem has four independent parameters that are generally set by the desired system geometry: the position of the projector, the position of the user, the position of the screen and the eyebox size. In this chapter our algorithm is explained through a generic automotive head-up display design process for the sake of simplicity, which has strict and challenging requirements for the system parameters [23].

## 4.1 Rotating microlenses for a high-gain screen

The key component of our direct projection HUD system is the embedded see-through screen. Microlens array (MLA) based eyebox (or exit pupil) expanders have been successfully demonstrated with color projectors [19]. Unlike diffractive optical element (DOE) based eyebox expanders, the microlenses expand the reflected light independent of the wavelength, so the sizes of the envelopes of the eyeboxes for each wavelength are the same [20], [21]. This offers very good color balance across the eyebox thus MLA based screens are desired for color projection.

With a planar reflective MLA, the reflection of the chief ray is governed by the usual Law of Reflection [24]. The eyebox is expanded about this central direction due to the curvature of the microlenses. Since the incidence angle of the light increases with increasing distance from the center of the screen, the eyebox created by each individual pixel is shifted by a different amount at the driver's position. Consequently, the full content on the screen can only be viewed from the overlapping region of all of the individual eyeboxes, which is smaller than the individual eyeboxes themselves.

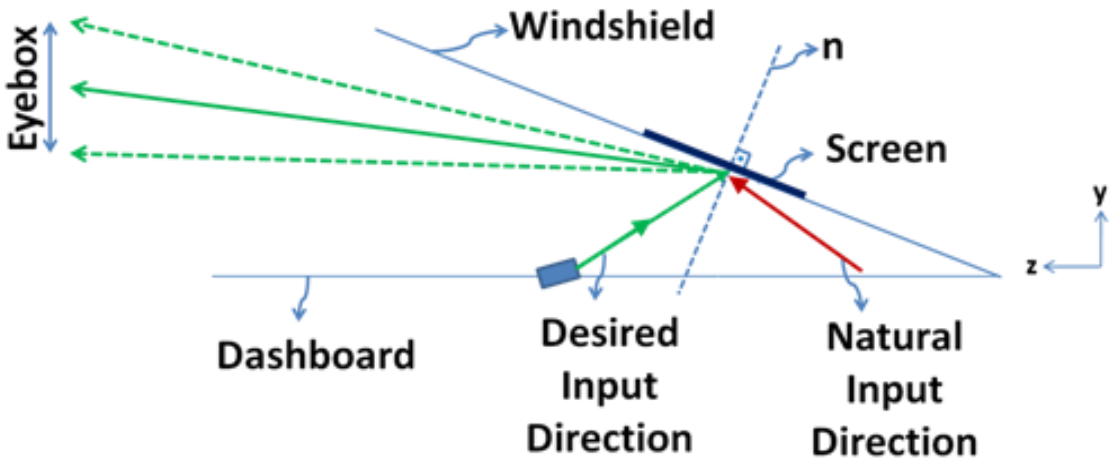


Figure 4.2: Natural input direction versus the desired input direction.

The natural input direction for the windshield embedded see-through screen, which is the incident beam direction that would relay the light to the driver's eye, is shown in Figure 4.2. Both the grazing angle of incidence onto the screen and the short projection distance available in most cars from this position are problematic. Projecting on an inclined surface causes keystone distortion but that can be compensated electronically in the video channel of the projector. The short projection distance results in too small an image to be of practical use for an automotive HUD. The easiest way to increase the projection distance is to place the projector closer to the driver’s side as indicated by the "desired input direction" in Figure 4.2. Moving from the natural input direction towards the desired input direction increases the shadowing effect, which will be discussed later; consequently there is a trade-off between the two input positions.

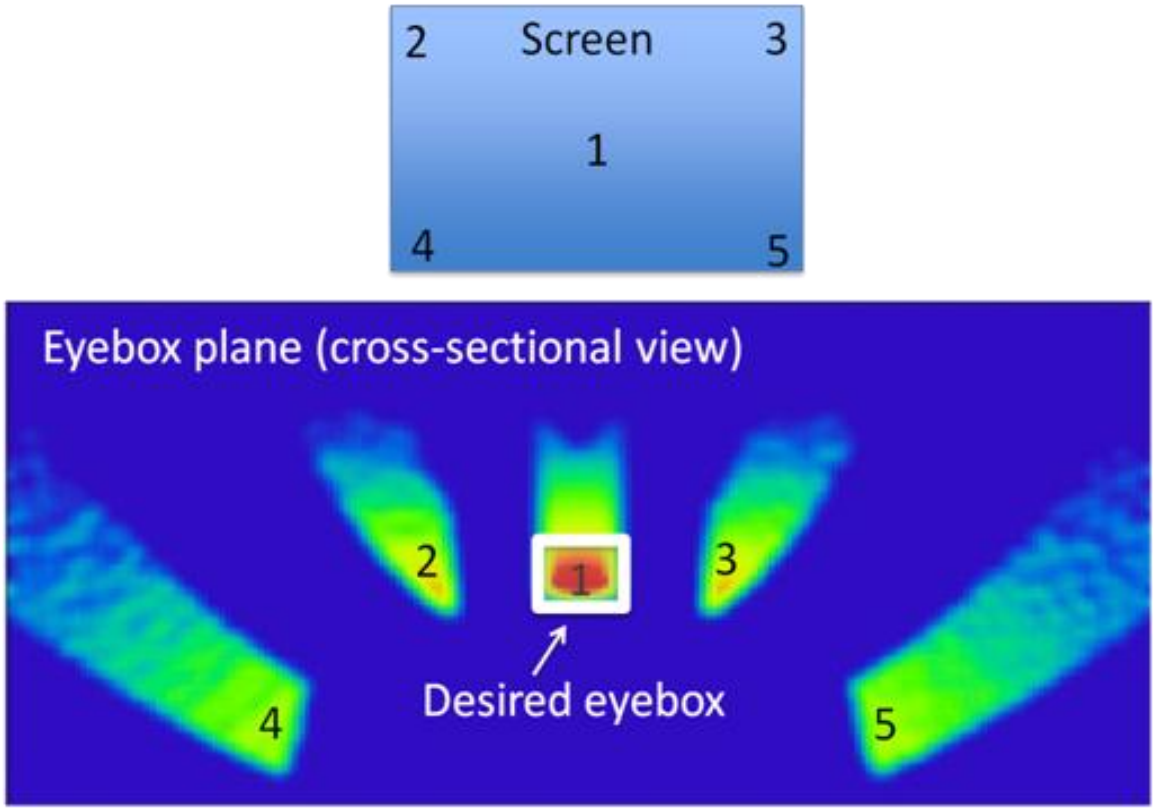


Figure 4.3: Simulated eyeboxes of an MLA screen for projecting from the natural input direction.

More importantly, the inclination of the screen results in an increased shift in each pixel's eyebox position. To illustrate this, we have simulated the four corners and the center of the planar MLA screen projected from the natural input direction for the geometry in Figure 4.2. The resulting eyeboxes have no overlapping region, as seen in Figure 4.3. This means that with the windshield embedded planar MLA there is no viewing position from which the driver would be able to view the entire projected image. In addition, each of the single pixel eyeboxes exhibits severe geometric distortion.

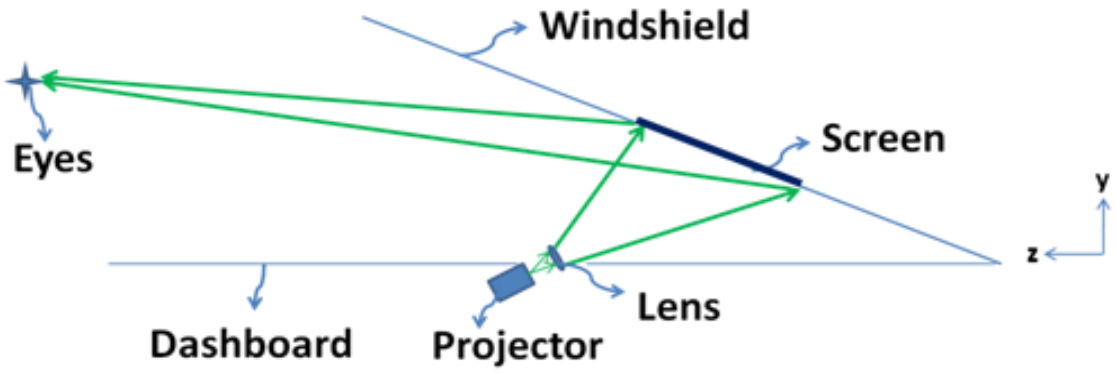


Figure 4.4: Using a lens to expand the scan cone of the projector.

Since the rotation angles of the microlenses are dependent on the system geometry such as the positions of the driver, the screen and the projector, we propose a design which we believe is suitable for a wide range of automobiles. In our design, we assumed that the angle between the z-axis and the windshield is 34°. The screen size is 175x87.5mm and the height of the center of the screen is 81mm from the dashboard. The driver is 1200mm away from the bottom of the windshield and the eyes are 250mm above the dashboard. The eyebox, which is centered between the driver's eyes, has a shape and size determined by the shape of the microlens' aperture and the radius of curvature, respectively. We used rectangular microlenses to produce a rectangular shaped eyebox. The 3.2mm radius of curvature of the microlenses has been selected to yield the desired eyebox size of about 30cm x 30cm at the driver's position.

With the specifications above, the proposed design is illustrated in Figure 4.4. The projector is placed on the dashboard with an angle such that the incident light at the center of the screen has perpendicular incidence. Alternatively, the projector could be buried within the dashboard since the projector engines are quite small for modern pico-projectors. It can be electrically connected to the vehicle to receive the necessary

information to be displayed. If there is not enough distance for the projector to illuminate the entire screen, the projection cone can be expanded by a small lens in front of the projector without adding much to the overall system size.

In our embedded see-through screen, we have designed an MLA with each microlens rotated about two axes, such that the incident beam is reflected towards the driver's eyes. In other words, the pointing of the microlenses steers the light coming from the projector towards the eyes of the driver while the curvature of microlenses expand the incident beam to create an eyebox. As a result, eyeboxes corresponding to every pixel on the screen overlap almost perfectly, so the available light is used more efficiently. This produces a useable eyebox where the individual pixel eyeboxes overlap, solving the problem shown in Figure 4.3, and because they overlap completely, it effectively increases the screen's brightness gain, giving more brightness than the partially overlapped case achieved by a planar MLA screen as in ref. [19]. Additionally, the tilting of each microlens, based on the specific geometry in a given car, compensates for the angle of the windshield from the position of the projector and therefore provides greater freedom of where to position the projector.

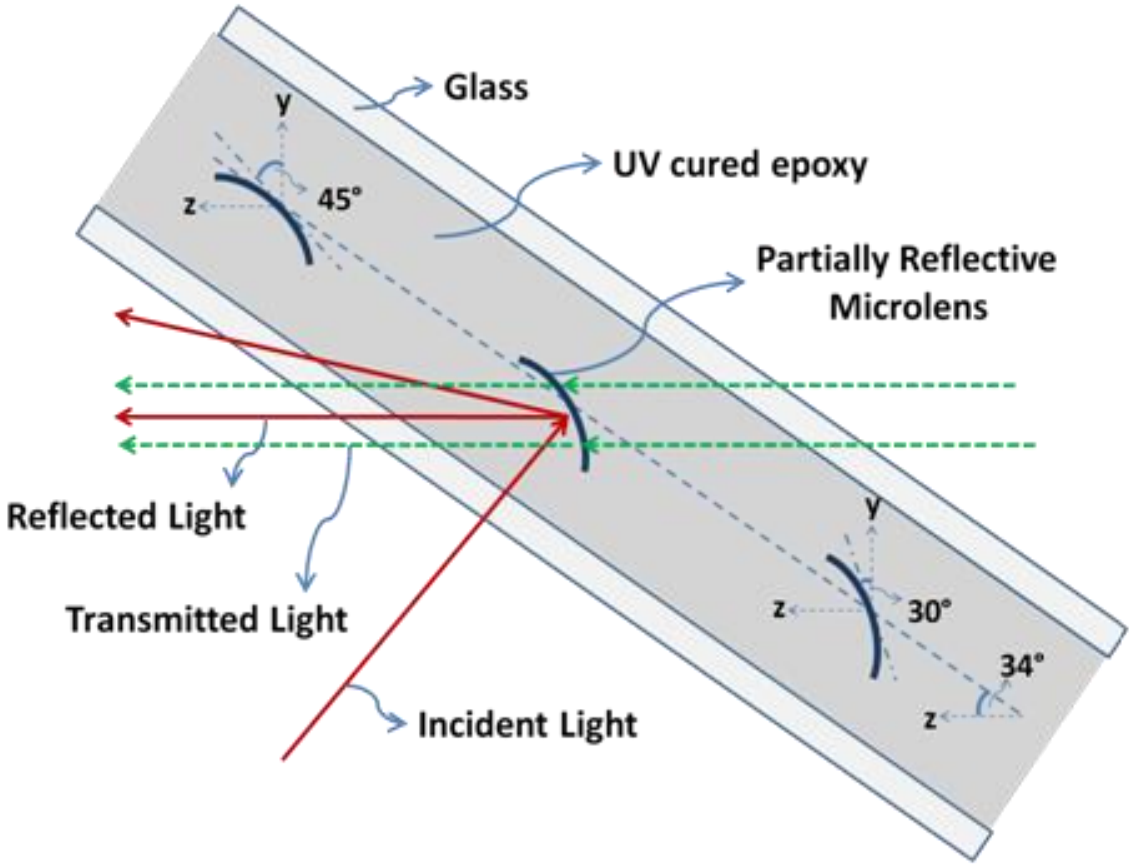


Figure 4.5: The rotated MLA screen structure.

Figure 4.5 illustrates the structure of the screen. The fabrication steps and the see-through screen operation principle were explained in Chapter 2.2.1. Unlike the planar MLA described in Chapter 0, the rotated MLA screen has microlenses oriented differently as a function of position on the screen.

As the screen has a faceted surface and it is used off-axis, one of the design challenges is to avoid the shadowing effect from adjacent microlenses that blocks the light coming from the lens immediately below as shown in Figure 4.6. Although the microlenses are 150μm tall, the MLA pitch is kept 300μm constant in both directions as illustrated in

Figure 4.7 to avoid shadowing, in other words the MLA pitch is kept constant but the aperture size is varied. As discussed in ref. [19], the MLA pitch optimal value is around 300um. The pitch is optimized using two constraints: (i) it should be smaller than the display pixel size, and (ii) it should be large enough to keep the diffraction order spacing at the eye smaller than the minimum pupil size to avoid intensity variations as the eye moves within the eyebox as discussed in Chapter 2.1.1.

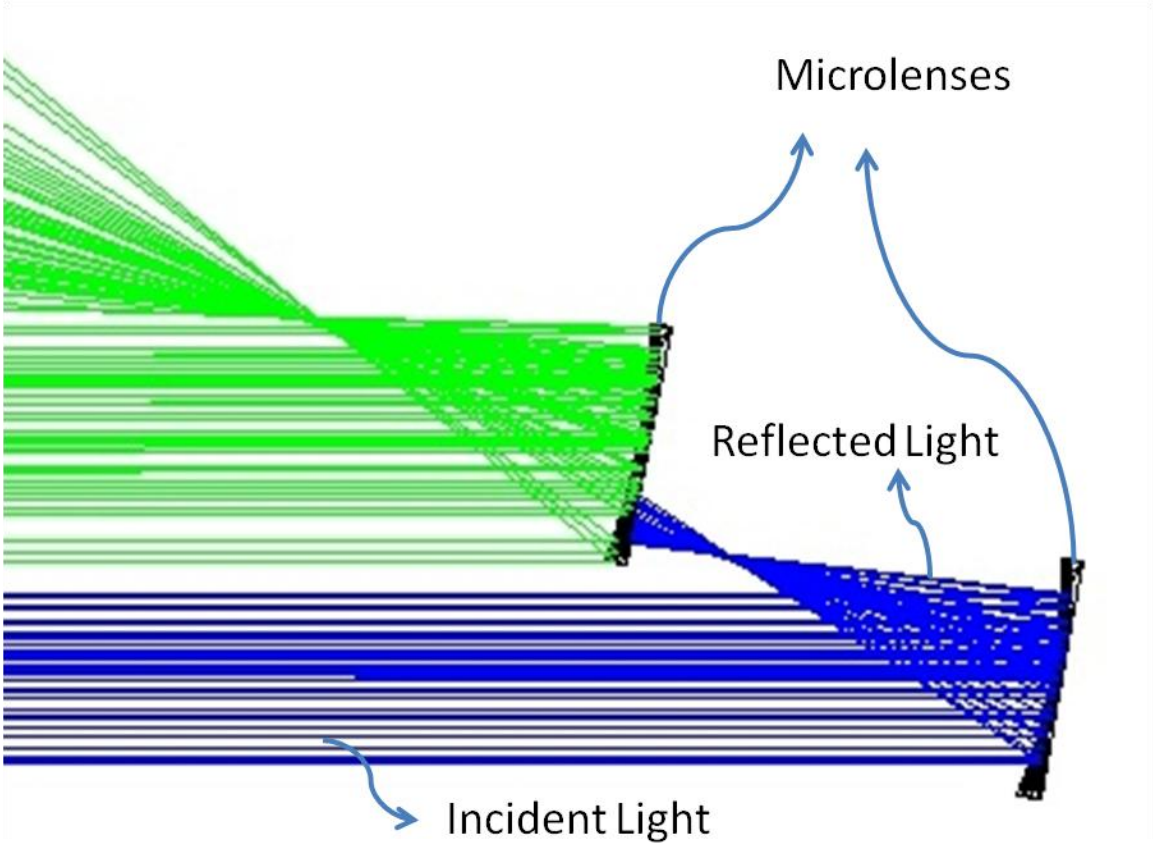


Figure 4.6: The shadowing effect of the adjacent microlenses.

With the given screen and microlens dimensions above, the resolution is approximately 583 x 292 pixels (calculated as screen size divided by microlens pitch). The maximum resolution of the laser scanning based pico-projector used in [19] was WVGA (850x480) pixels. The additional resolution of the projector provides overhead for use in electronically correcting for keystone and other distortions.

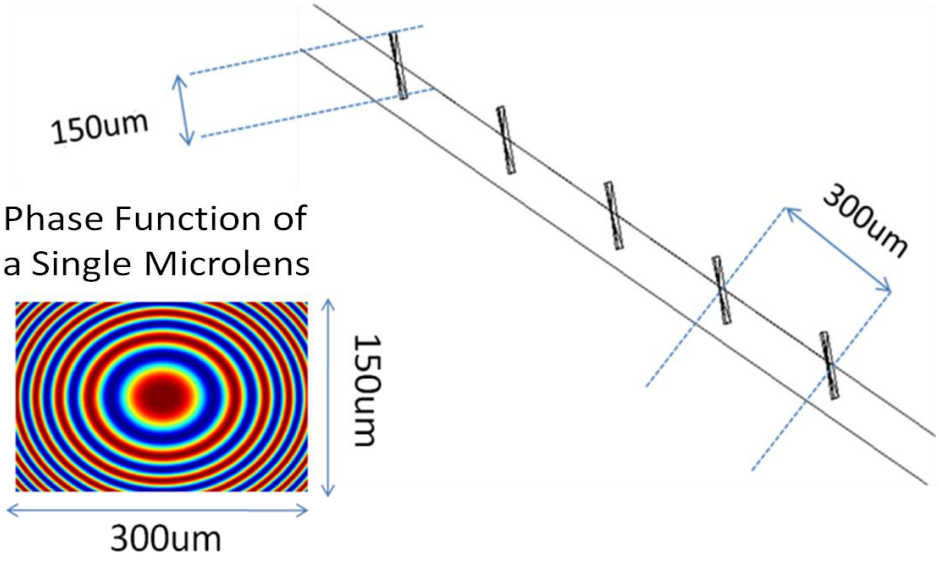


Figure 4.7: The Zemax model of the rotated MLA screen. Although the microlenses are 150μm tall, the MLA pitch in the vertical direction is set to 300μm to prevent shadowing.

As discussed in Chapter 2.2.2 in greater detail, a broadband metal or dielectric coating can be used on the MLA with any projector that has a broadband or narrowband light source, such as LED or laser based projectors. Notch coatings that reflect almost 100% of the desired wavelengths and transmit 100% of the rest of the spectrum may provide higher performance with the screen. The condition on the OPD generated due to the thickness of the reflective coating to be less than $\lambda/4$ is also valid with the rotated MLA, as discussed in Chapter 2.2.2.

### 4.1.1 Calculating the rotation angles of the microlenses

We calculated the rotation angles of the microlenses using the following methodology: Since the tilting of the microlenses is intended to center the individual pixel eyeboxes between the driver's eyes, we begin by treating the microlenses as planar micro-mirrors. We then calculate their rotations about the x and y axes to steer the incoming light from the projector towards the driver. Finally, we convert the rotated flat micro-mirrors into microlenses to expand the light to create the eyebox. The most important part of our design is the calculation of the rotation angles of the microlenses to reflect the incident beam towards the driver's eyes. The rotation angles are calculated based on the positions of the projector, the driver, and the individual microlenses, using the method described below. In this paper, we assumed that the windshield was planar as a representative example of the calculation procedure. Since the microlens rotation angles are calculated based on the position of the individual microlenses, our algorithm can calculate the rotation angles based on the surface profile of any particular windshield.

Since the microlenses are buried in an index-matched layer, the incident and reflected light are subject to refraction due to the refractive index difference between the windshield and the surrounding air, as illustrated in Figure 4.8a. Thus, the problem of finding the aiming point on the interface to get the light crossing the desired point in the other medium must be included in the calculations. Figure 4.8b illustrates the details of refraction at the glass interface. Equations below are used to calculate the vectors $\mathbf{Vi_1}$ and $\mathbf{Vr_1}$ to find the path from projector to micro-mirror. The path from the micro-mirror to the driver's eye is calculated in a similar manner by applying the same set of equations to find $\mathbf{Vi_2}$ and $\mathbf{Vr_2}$ in Figure 4.8a.

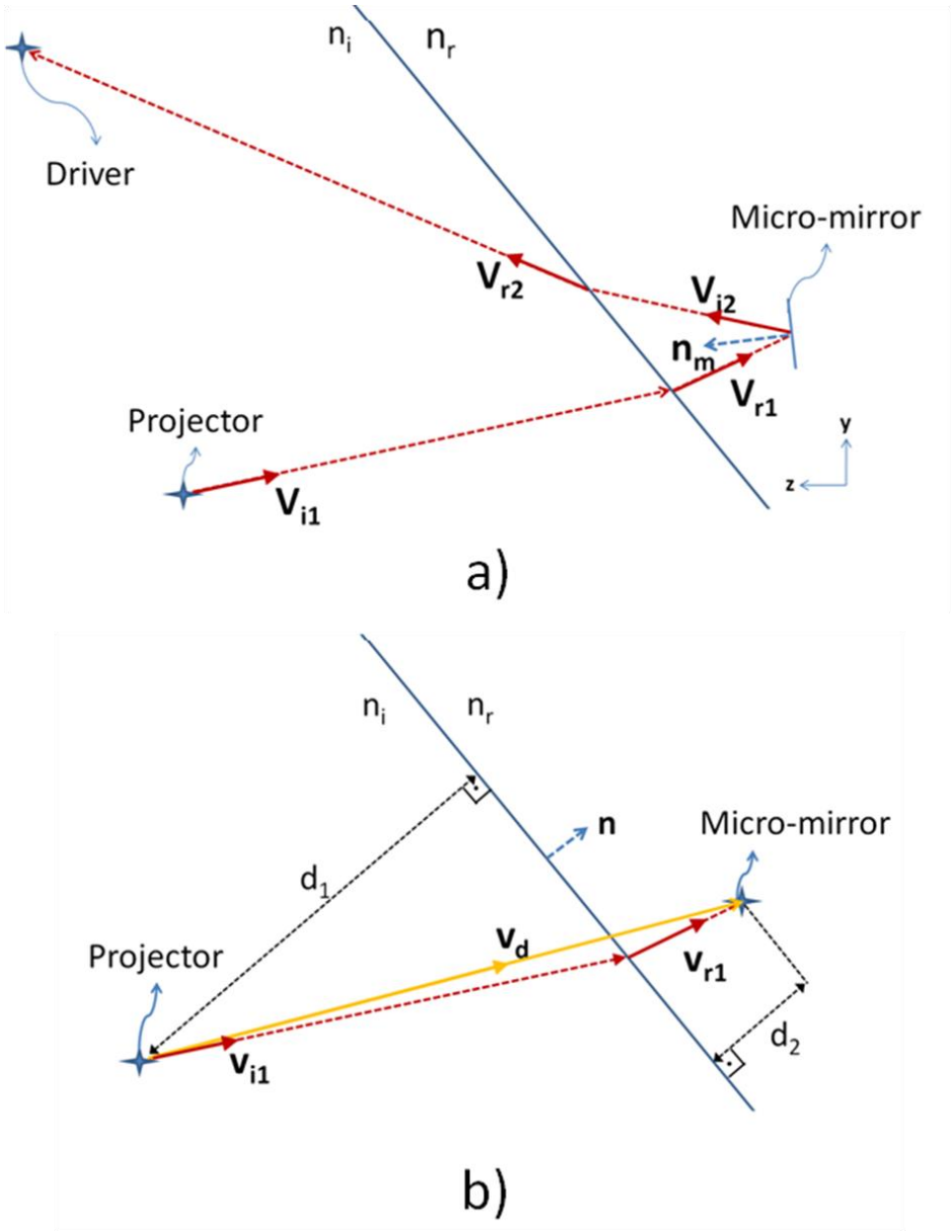


Figure 4.8: The illustration of the geometry for calculating of the rotation angles.

Snell's Law in vector form is shown in Eq. (4-1), where **n** is the unit surface normal vector of the interface, η is the ratio of the refractive indices $n_i / n_r$, $\mathbf{v_{i1}}$ and $\mathbf{v_{r1}}$ are the unit vectors along the incident and refracted light respectively [26]. As both the incident and refracted vectors are not known, a second equation is needed to obtain two equations with two unknowns. A weighted sum of $\mathbf{v_{i1}}$ and $\mathbf{v_{r1}}$ should result in the desired vector $\mathbf{v_d}$, which is the vector between the desired initial and final points, as illustrated in Figure 4.8b. The weights of the vectors should be selected as in Eq.(4-2), where $d_1$ and $d_2$ are the distances of the initial and final points to the interface plane and $(\mathbf{v_{i1}} \cdot \mathbf{n})$ and $(\mathbf{v_{r1}} \cdot \mathbf{n})$ are the dot products of the incident and refracted unit vectors with the interface surface normal, respectively. Eq. (4-3) is obtained by solving Eq. (4-1) and Eq. (4-2) together, where $(\mathbf{v_{i1}} \cdot \mathbf{n})$ is the only independent unknown. As the dot product is a scalar quantity, the incident vector $\mathbf{v_{i1}}$ is expressed as a single variable function of $(\mathbf{v_{i1}} \cdot \mathbf{n})$. We know that $\mathbf{v_{i1}}$ is a unit vector so its norm should be equal to one. To get the correct value of $(\mathbf{v_{i1}} \cdot \mathbf{n})$, f(x) in Eq. (4-4) is minimized iteratively using the Newton-Raphson method [27], where x denotes $(\mathbf{v_{i1}} \cdot \mathbf{n})$.

$$\mathbf{v_{r1}} = \left( sign(\mathbf{v_{i1}} \bullet \mathbf{n}) \sqrt{1 - \eta^2 + \eta^2 (\mathbf{v_{i1}} \bullet \mathbf{n})^2} - (\mathbf{v_{i1}} \bullet \mathbf{n}) \eta \right) \mathbf{n} + \eta \mathbf{v_{i1}} \tag{4-1}$$

$$\mathbf{v_d} = \frac{d_1}{\mathbf{v_{i1}} \bullet \mathbf{n}} \mathbf{v_{i1}} + \frac{d_2}{\mathbf{v_{r1}} \bullet \mathbf{n}} \mathbf{v_{r1}} \tag{4-2}$$

$$\mathbf{v_{i1}} = \frac{\mathbf{v_d} - d_2\left(1 - \dfrac{\eta(\mathbf{v_{i1}} \bullet \mathbf{n})}{\sqrt{1-\eta^2+\eta^2(\mathbf{v_{i1}} \bullet \mathbf{n})^2}}\right)\mathbf{n}}{\dfrac{d_1}{(\mathbf{v_{i1}} \bullet \mathbf{n})} + \dfrac{\eta d_2}{\sqrt{1-\eta^2+\eta^2(\mathbf{v_{i1}} \bullet \mathbf{n})^2}}} \tag{4-3}$$

$$f(x) = \left\|\mathbf{v_{i1}}\right\| - 1 \tag{4-4}$$

Once $\mathbf{v_{i1}}$ is obtained by plugging in the computed value of $(\mathbf{v_{i1}} \cdot \mathbf{n})$ in Eq. (4-3), $\mathbf{v_{r1}}$ can be calculated using Eq. (4-1). This procedure is followed two times for each micro-mirror: for finding the unit incident and refracted vectors from the projector to the micro-mirror and from the micro-mirror to the driver as shown in Figure 4.8a as $\mathbf{Vi_1}$, $\mathbf{Vr_1}$, $\mathbf{Vi_2}$, $\mathbf{Vr_2}$, respectively. Surface normal of the micro-mirror should be calculated such that when $\mathbf{Vr_1}$ is the incident unit vector, $\mathbf{Vi_2}$ should be the reflected unit vector. Eq. (4-5) gives the reflected unit vector $\mathbf{Vi_2}$, when a unit vector $\mathbf{Vr_1}$ is incident on a surface with surface normal $\mathbf{n_m}$ [26]. In our case, we know the incident and reflected vectors and we need the surface normal vector. Using the fact that angle of incidence is equal to the angle of reflection, Eq.(4-5) can be transformed into Eq. (4-6), which gives the surface normal vector when incident and reflected vectors are known [24].

After we find the surface normal vector, the required rotation angles can be calculated by solving the rotation matrix shown in Eq. (4-7), where θ and ϕ are the rotations about the x and y axes, respectively. $x_m$, $y_m$, $z_m$ in Eq. (4-7) are the components of the vector $\mathbf{n_m}$.

Unrotated micro-mirrors are assumed to have unit surface normal vectors parallel to the z-axis. (The coordinate axes are shown in Figure 4.4)

$$\mathbf{v}_{\mathbf{i}2} = \mathbf{v}_{\mathbf{r1}} - 2(\mathbf{v}_{\mathbf{r1}} \bullet \mathbf{n}_{\mathbf{m}})\mathbf{n}_{\mathbf{m}} \tag{4-5}$$

$$\mathbf{n}_{\mathbf{m}} = \frac{\mathbf{v}_{\mathbf{r1}} - \mathbf{v}_{\mathbf{i2}}}{\sqrt{2(1-(\mathbf{v}_{\mathbf{i2}} \bullet \mathbf{v}_{\mathbf{r1}}))}} \tag{4-6}$$

$$\begin{bmatrix} \cos\varphi & 0 & \sin\varphi \\ \sin\varphi\sin\theta & \cos\theta & -\cos\varphi\sin\theta \\ -\sin\varphi\cos\theta & \sin\theta & \cos\varphi\cos\theta \end{bmatrix} \begin{bmatrix} 0 \\ 0 \\ 1 \end{bmatrix} = \begin{bmatrix} x_m \\ y_m \\ z_m \end{bmatrix} \tag{4-7}$$

$$\varphi = \sin^{-1}(x_m) \tag{4-8}$$

$$\theta = \tan^{-1}(-\frac{y_m}{z_m}) \tag{4-9}$$

MATLAB was used to calculate the rotation angles for each micro-mirror on the screen using the method described above. Figure 4.9 shows the 2D contour plot of the magnitude of the compound rotation angles for the design in Figure 4.4 as a function of micro-mirror position, that is, $[\theta^2 + \varphi^2]^{1/2}$. The tilt direction is normal to the contour lines.

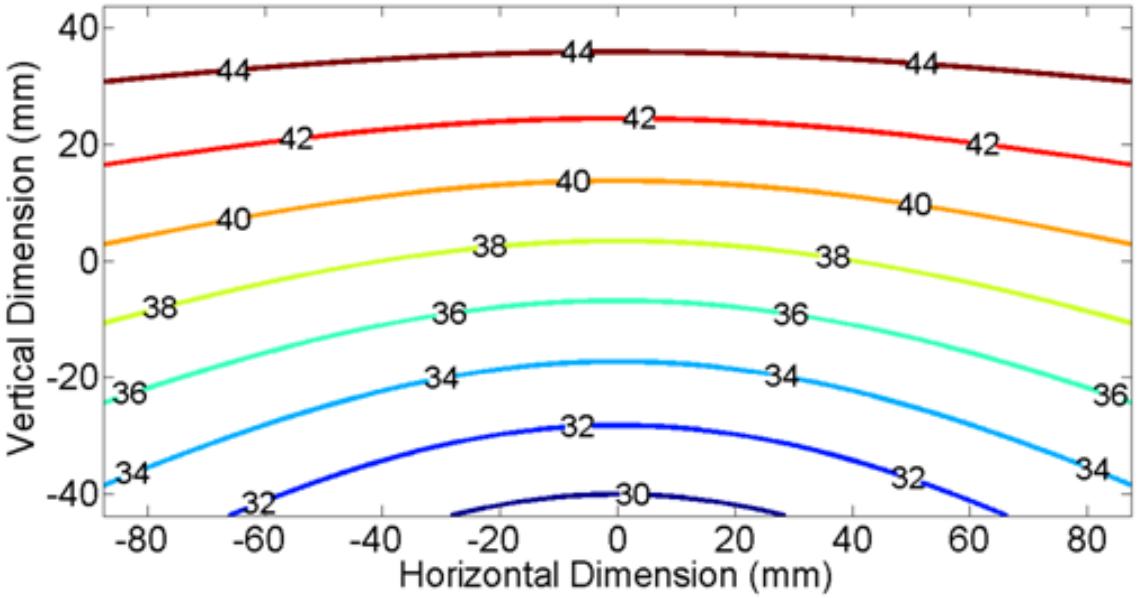


Figure 4.9: The calculated contour plot of the rotation angles ($[\theta^2 + \varphi^2]^{1/2}$).

### 4.1.2 Rotated microlens array fabrication

Fabrication of MLAs with individually rotated microlenses remains as a challenge. We investigated possible fabrication technologies and based on our private communications with different companies there are two different options to fabricate such a screen: precision diamond turning and pulsed laser ablation. According to our private communications with diamond turning companies the machining process for a 10cm x 20cm screen mold would take more than 10 days, which is very expensive and risky, as many things can go wrong during the machining process, but in principle such a rotated MLA screen can be fabricated using this technology.

The second fabrication technology, pulsed laser ablation by EMPA Crealas, is a more reliable option [28][29] [30]. Any 3D surface profile can be fabricated on large substrates. Figure 4.10 illustrates the fabrication steps of pulsed laser ablation technique. First the

desired feature is divided into cross-sections and a lithography mask consisting of consecutive cross-section shapes is fabricated. The substrate is moved under the lithography mask with discrete steps and the substrate is ablated using laser pulses. As the substrate moves the desired features are fabricated layer by layer.

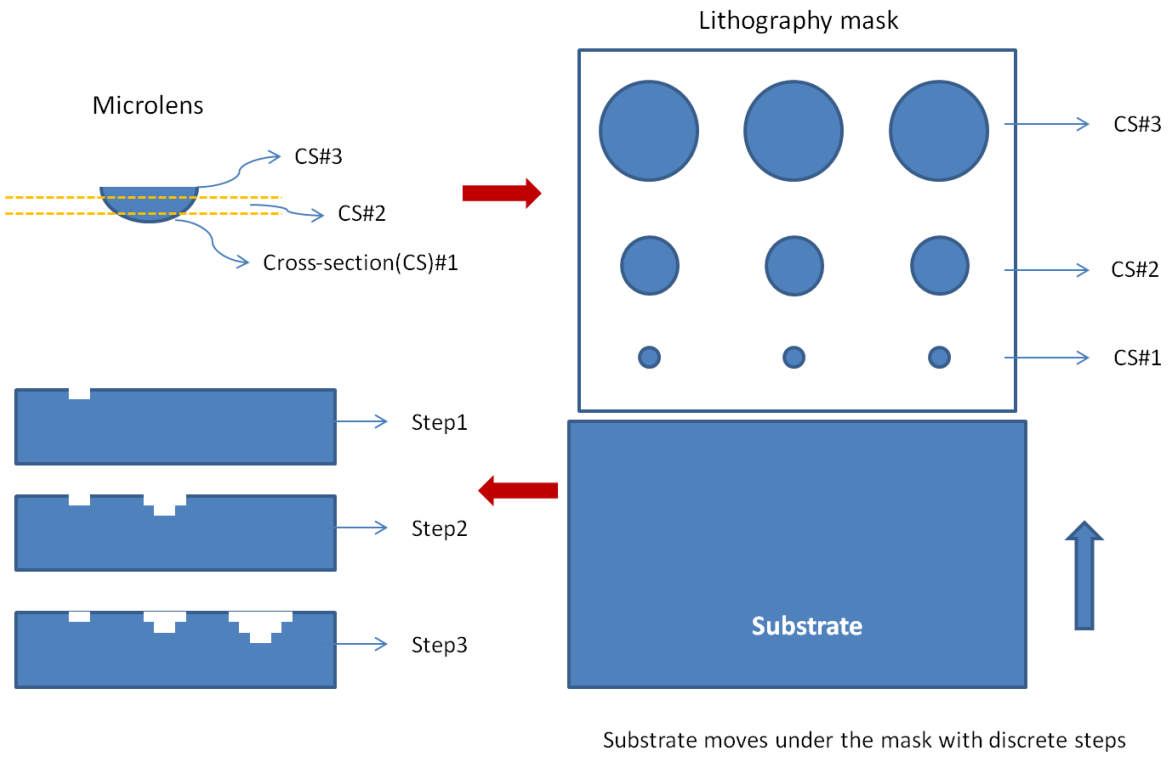


Figure 4.10: Fabrication steps of the rotated MLA screen.

## 4.2 Ray optics simulation results

We used five sample points on the screen to simulate the system in Zemax, one from each corner and one from the center. The side view of the system is shown in Figure 4.11, which shows the focusing characteristic of our screen with flat micro-mirrors. Once the flat micro-mirrors are converted into microlenses, the resulting eyeboxes for each point on the

screen overlap almost perfectly. This maximizes the gain of the screen by steering most of the light to the fully overlapped region of the eyeboxes where the complete field of view can be seen.

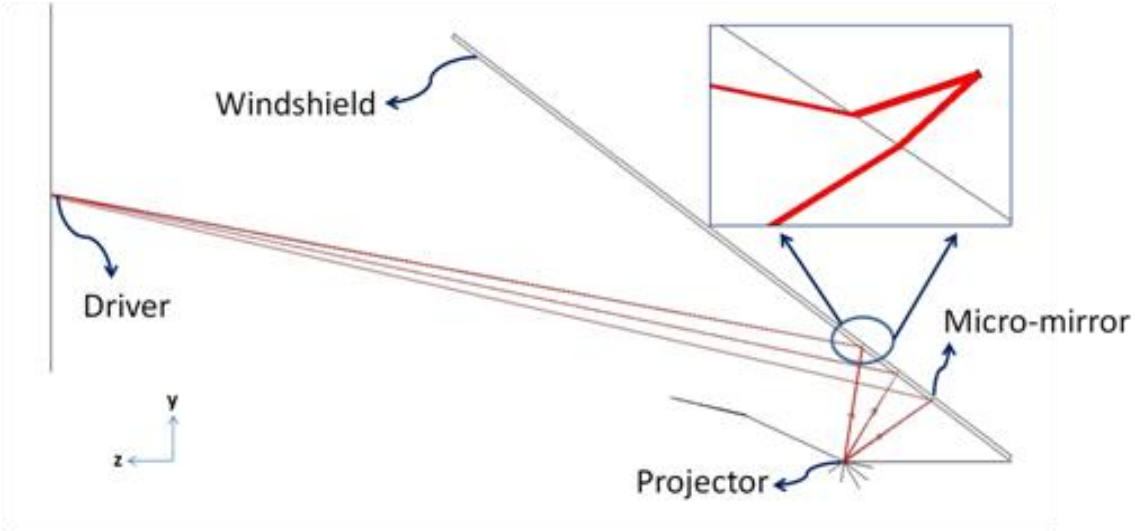


Figure 4.11: The side view of the Zemax model of the system in Figure 4.4 showing the focusing characteristic of our rotated MLA screen.

We used a 635nm, collimated Gaussian beam as the source in a Zemax model for simulating the screen. In Figure 4.13, the eyeboxes for the five selected points are shown at the driver's position. There is some geometric distortion due to the off-axis operation of the microlenses which results in an elongation of the eyebox. The effects of the chromatic aberrations were checked by simulating the modeled system using the Zemax software. The simulation scheme is as follows: The most off-axis illuminated microlens in the screen is simulated with three laser wavelengths of 645nm, 532nm and 445nm of equal power. An eye model with 3mm pupil size is placed in the driver's position, which focused the light on a color detector. The dispersion characteristics for the materials used were already modeled in Zemax. Figure 4.12a shows the image corresponding to monochromatic

illumination (λ=645nm). Figure 4.12b shows the image for all three wavelengths. As no shifting is observed at the retina for different colors, it is concluded that the windshield embedded screen has negligible chromatic aberrations.

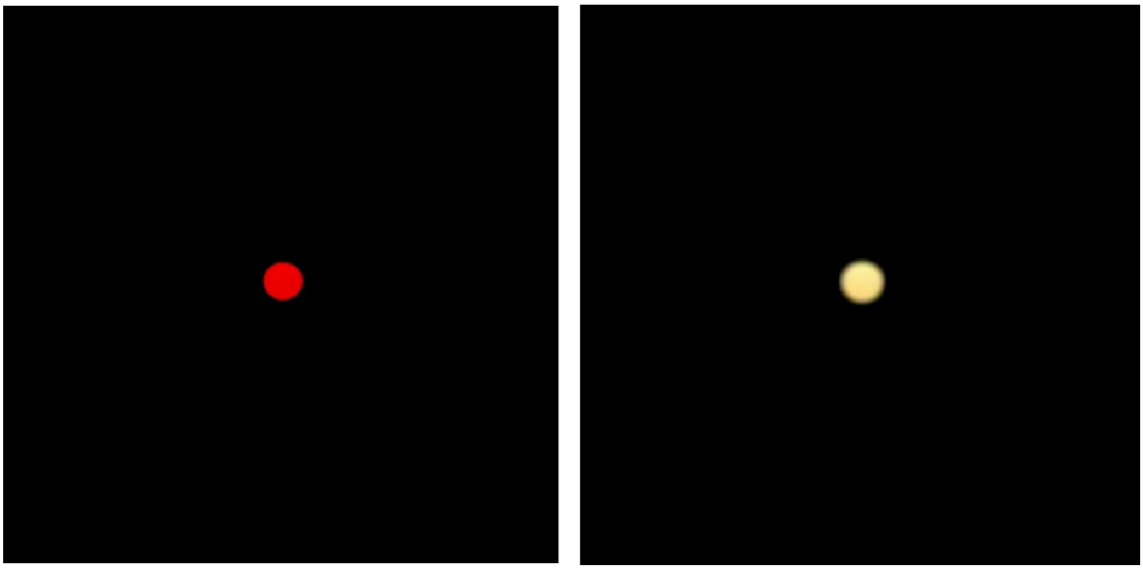


Figure 4.12: The simulation of the chromatic aberrations in the rotated MLA screen.

The gain of the MLA screen, which is the ratio of the intensity compared to that obtained with a Lambertian scatterer, is calculated as 69. The perceived brightness within the eyebox using a 20-lumen projector is 7171cd/$m^2$, assuming 50% reflective screen. This exceptional brightness can be utilized in two different ways: the projector power can be lowered, consequently the energy dissipation of the whole system is lowered or, the reflectivity of the screen can be decreased hence the transparency is enhanced, making it even more difficult to distinguish the screen from the windshield.

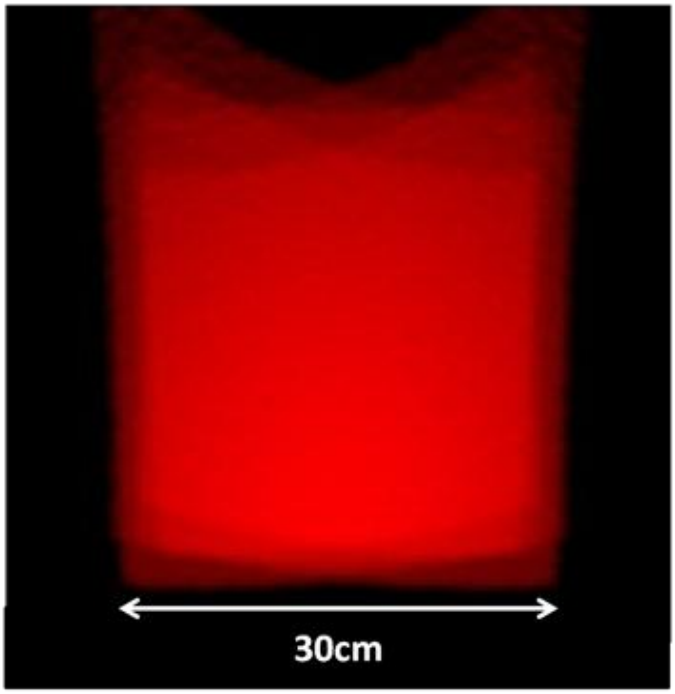


Figure 4.13: The true color simulation of the eyebox for the system in Figure 4.4.

The design target for the eyebox width is 250mm. The horizontal and vertical cross-sections of the simulated eyebox are shown in Figure 4.14. As the eyes are oriented horizontally, the variations in the horizontal cross-section are perceived more easily. The horizontal cross-section of the eyebox is quite uniform, so that the perceived brightness is almost equal for both eyes and it is sufficiently large for comfortable operation. The vertical cross-section shows the margin of the system to accommodate different heights of the drivers.

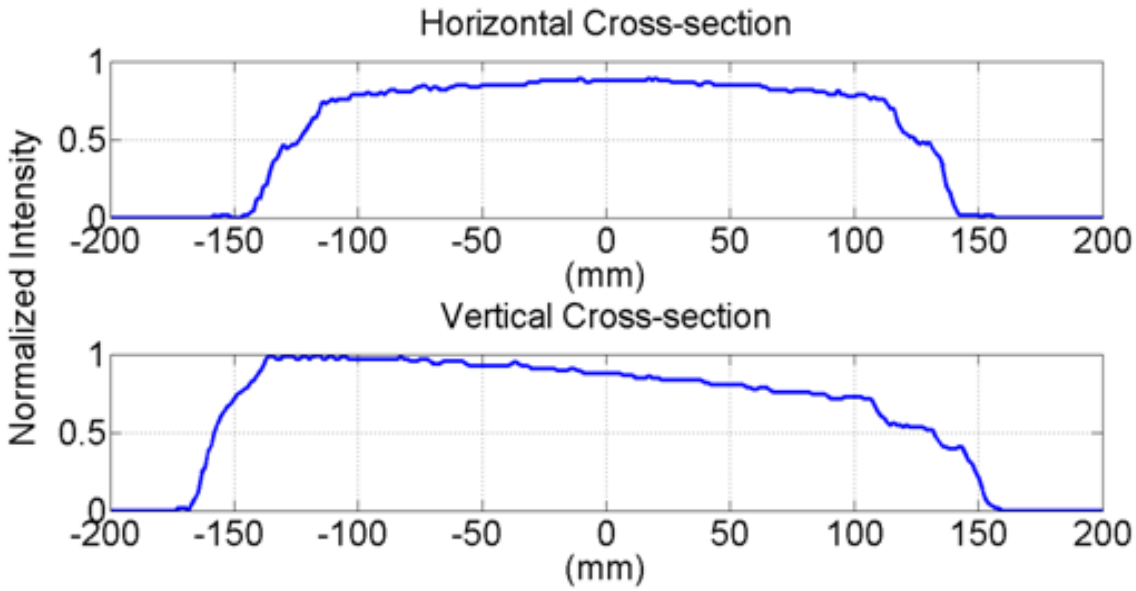


Figure 4.14: The simulated horizontal and vertical intensity cross-sections of the eyebox.

# 5 CONCLUSION

In this thesis, design methodologies, simulation and experimental results for three different MLA based screens have been discussed. The relationship between the display parameters, such as the brightness, eyebox size and image quality and the screen parameters, such as the gain, MLA pitch, and radius of curvature, have been established. The refractive index-matched see-through screen structure has been introduced and the effect of the semi-reflective coating has been investigated. It has been found that the total optical path difference due to the coating should be less than a quarter of the wavelength for diffraction limited operation of the screen in the transmission mode. The designed screen has been simulated in Zemax and fabricated with various reflective coatings. The singe MLA screen has a gain of 3 compared to a Lambertian screen. It has been demonstrated in a real car as an inexpensive and compact alternative to the existing virtual HUD systems in cars.

A reflective dual MLA screen with a gain of 9 has been introduced and its operation principle has been explained both theoretically and by using simulations. The dual MLA screen has been compared to the single MLA screen in terms of screen gain and eyebox uniformity. The fabricated screen was successfully demonstrated as a high gain display for pico-projectors but it couldn't be utilized as an HUD screen in cars due to ghost image problems.

The highest gain is achieved using a unique rotated MLA screen where each microlens in the array is rotated such that the chief rays of the incident light are focused exactly on the user's eyes. The screen should be custom designed specifically for different applications, which can be transparent or opaque depending on the requirements. The

design procedure has been explained and the simulation results have been discussed. With this screen technology it is possible to achieve gains on the order of 100.

## BIBLIOGRAPHY


[1] Ryer, Alex, and Visible Light. "Light measurement handbook." (1997).

[2] Chellappan, Kishore V., Erdem Erden, and Hakan Urey. "Laser-based displays: a review." Applied optics 49.25 (2010): F79-F98.

[3] Goodman, J. W. "Some fundamental properties of speckle." JOSA 66.11 (1976): 1145-1150.

[4] Goodman, J.W., [Introduction to Fourier Optics, 2nd edition], McGraw-Hill Book Co., New York, 207, (1996

[5] Hass, G., and J. E. Waylonis. "Optical constants and reflectance and transmittance of evaporated aluminum in the visible and ultraviolet." JOSA 51.7 (1961): 719-722.

[6] M. Estribeau and P. Magnan, "Fast MTF measurement of CMOS imagers using ISO 12233 slanted edge methodology," Proc. SPIE 5251, 243-251 (2004).

[7] Canny, John. "A computational approach to edge detection." *Pattern Analysis and Machine Intelligence, IEEE Transactions on* 6 (1986): 679-698.

[8] Pearson, Karl. "LIII. On lines and planes of closest fit to systems of points in space." *The London, Edinburgh, and Dublin Philosophical Magazine and Journal of Science* 2.11 (1901): 559-572.

[9] Voelz, David George, "Computational Fourier Optics: A MATLAB Tutorial" SPIE, 2011.

[10] Smith, Warren J. *Modern optical engineering*. Tata McGraw-Hill Education, 2000.

[11] Aleksandar D. Rakić. *"Algorithm for the determination of intrinsic optical constants of metal films: application to aluminum"*, Applied. Optics. 34, 4755-4767 (1995)

[12] M. J. Kidger, Fundamental Optical Design, SPIE Press, Bellingham, WA (2001).

[13] Sankur, Haluk O., and M. Edward Motamedi. "Micro-optics development in the past decade." Micromachining and Microfabrication. International Society for Optics and Photonics, 2000.

[14] Gale, Michael T., et al. "Fabrication of continuous-relief micro-optical elements by direct laser writing in photoresists." Optical Engineering 33.11 (1994): 3556-3566.

[15] Hessler, Thomas, et al. "Analysis and optimization of fabrication of continuous-relief diffractive optical elements." Applied optics 37.19 (1998): 4069-4079.

[16] O'Neill, Feidhlim T., and John T. Sheridan. "Photoresist reflow method of microlens production Part I: Background and experiments." Optik-International Journal for Light and Electron Optics 113.9 (2002): 391-404.

[17] Schilling, Andreas, et al. "Surface profiles of reflow microlenses under the influence of surface tension and gravity." Optical Engineering 39.8 (2000): 2171-2176.

[18] Baranski, Maciej, et al. "Fabrication of 100% fill factor arrays of microlenses from silicon molds." Proc. of SPIE Vol. Vol. 8428. 2012.

[19] M.K. Hedili, M. O. Freeman, H. Urey, "Microstructured head-up display screen for automotive applications", Proc. SPIE 8428, (2012).

[20] H. Urey and K. D. Powell, "Microlens-array-based exit-pupil expander for full-color displays", Applied Optics , vol. 44, pp.4930 - 4936 , (2005).

[21] H. Urey, "Diffractive Exit-Pupil Expander for Display Applications," Applied Optics, Vol. 40, No. 32, p.5840-5851, (2001).

[22] Oppenheim, Alan V., Ronald W. Schafer, and John R. Buck. *Discrete-time signal processing*. Vol. 5. Upper Saddle River: Prentice Hall, 1999.

[23] Hedili, M. Kivanc, Mark O. Freeman, and Hakan Urey. "Microlens array-based high-gain screen design for direct projection head-up displays." Applied optics52.6 (2013): 1351-1357.

[24] F. L. Pedrotti, L. M. Pedrotti, L.S. Pedrotti, *Introduction to Optics, 3rd Edition*, (Pearson Prentice Hall, New Jersey, 2007).

[25] Pedder, J. E. A., et al. "Pulsed laser ablation for volume fabrication of micro-optical arrays on large-area substrates." MOEMS-MEMS 2007 Micro and Nanofabrication. International Society for Optics and Photonics, 2007.

[26] D. Fontijne and L. Dorst, "Modeling 3D Euclidean Geometry", IEEE Computer Graphics and Applications vol.23 n.2, 68-78, (2003).

[27] J.E. Dennis and R.B. Schnabel, Numerical Methods for Unconstrained Optimization and Nonlinear Equations, (Prentice-Hall, 1983), Chap.2.

[28] Pedder, J. E. A., et al. "Pulsed laser ablation for volume fabrication of micro-optical arrays on large-area substrates." MOEMS-MEMS 2007 Micro and Nanofabrication. International Society for Optics and Photonics, 2007.

[29] Boehlen, Karl L., Ines B. Stassen Boehlen, and Ric M. Allott. "Advanced laser micro-structuring of super-large-area optical films." MOEMS-MEMS Micro & Nanofabrication. International Society for Optics and Photonics, 2005

[30] Boehlen, Karl L., and Ines B. Stassen Boehlen. "Laser micromachining of high-density optical structures on large substrates." Lasers and Applications in Science and Engineering. International Society for Optics and Photonics, 2004.